

DISK: DIFFERENTIALLY PRIVATE OPTIMIZER WITH SIMPLIFIED KALMAN FILTER FOR NOISE REDUCTION

Xinwei Zhang^{1*} Zhiqi Bu^{2†} Borja Balle³ Mingyi Hong⁴ Meisam Razaviyayn^{1*}
Vahab Mirrokni⁵

¹University of Southern California, ²Amazon, ³DeepMind, ⁴University of Minnesota,

⁵Google Research

ABSTRACT

Differential privacy (DP) offers a robust framework for safeguarding individual data privacy. To utilize DP in training modern machine learning models, differentially private optimizers have been widely used in recent years. A popular approach to privatize an optimizer is to clip the individual gradients and add sufficiently large noise to the clipped gradient. This approach led to the development of DP optimizers that have comparable performance with their non-private counterparts in fine-tuning tasks or in tasks with a small number of training parameters. However, a significant performance drop is observed when these optimizers are applied to large-scale training. This degradation stems from the substantial noise injection required to maintain DP, which disrupts the optimizer’s dynamics. This paper introduces DiSK, a novel framework designed to significantly enhance the performance of DP optimizers. DiSK employs Kalman filtering, a technique drawn from control and signal processing, to effectively denoise privatized gradients and generate progressively refined gradient estimations. To ensure practicality for large-scale training, we simplify the Kalman filtering process, minimizing its memory and computational demands. We establish theoretical privacy-utility trade-off guarantees for DiSK and demonstrate provable improvements over standard DP optimizers like DPSGD in terms of iteration complexity upper-bound. Extensive experiments across diverse tasks, including vision tasks such as CIFAR-100 and ImageNet-1k and language fine-tuning tasks such as GLUE, E2E, and DART, validate the effectiveness of DiSK. The results showcase its ability to significantly improve the performance of DP optimizers, surpassing state-of-the-art results under the same privacy constraints on several benchmarks.

1 INTRODUCTION

Data privacy has become one of the major concerns in modern machine learning systems. Differential Privacy (DP), with its rigorous mathematical foundation, offers a powerful solution. DP provides a framework for developing training algorithms that safeguard the privacy of individuals’ data used to train machine learning models. Among various algorithms, Differentially Private Stochastic Gradient Descent (DPSGD) (Abadi et al., 2016) and its variants (Li et al., 2021; Yu et al., 2021; Tang et al., 2024) have emerged as popular choices for training various models, including computer vision (De et al., 2022) and language models (Bu et al., 2023; 2024). These algorithms inject noise into the training process to guarantee privacy. However, this noise injection often comes at a significant cost to model performance, limiting the widespread adoption of DP optimizers (Jayaraman & Evans, 2019). For example, (McMahan et al., 2018; De et al., 2022) observed that DP training led to a 15% drop in model accuracy on the Reddit dataset and a 30% drop on CIFAR-10 compared to non-private training. This challenge has limited the application of DP optimizers primarily to small models or parameter-efficient fine-tuning, as highlighted by (Li et al., 2021).

Many recent works aim to improve differentially private (DP) training performance. These include applying low-pass filters to separate gradients from noise (Zhang et al., 2024a), injecting correlated noise with algorithms like DP-FTLR (Koloskova et al., 2023; Choquette-Choo et al., 2024), using sharpness-aware minimization for flatter loss landscapes that are less sensitive to DP noise (Park

*xinweiz, razaviya@usc.edu, [†]This work is not affiliated with Zhiqi Bu’s position at Amazon.

et al., 2023), adaptive clipping (Andrew et al., 2021; Lin et al., 2022; Hu et al., 2021), and model structure optimization (Bu et al., 2024; Papernot et al., 2021; De et al., 2022). However, these methods often require extra memory, lack theoretical guarantees, or have limited applicability. Therefore, there is a strong demand to design a new approach that 1) is memory and computation efficient for implementation, 2) has a theoretical guarantee, and 3) is compatible with a wide range of existing DP optimization algorithms and models. To meet this demand, we leverage the Kalman filter, a tool from control theory, to improve gradient estimates in DP optimization. We further simplify our algorithm for memory and computational efficiency, while maintaining theoretical grounding and broad compatibility with existing DP algorithms and models.

The tools in signal processing and control theory have been leveraged to design novel optimization algorithms. In the context of DP optimization, the error-feedback approach has been adopted to reduce the bias caused by the clipping operation (Zhang et al., 2024b); the low-pass and high-pass filters have been used to separate the gradient from the DP noise (Zhang et al., 2024a; Koloskova et al., 2023; Choquette-Choo et al., 2024); the low-pass spatial filter, including Gaussian and Laplace filters have been used to smooth the privatized model or gradient across dimensions (Wang et al., 2020a; 2021; Liu et al., 2022). These methods effectively improve DP optimizers’ performance.

1.1 CONTRIBUTIONS

Our approach centers on constructing a dynamic system where the gradient serves as its state. We treat the privatized gradient as a noisy observation of the true gradient within this system. By applying a Kalman filter, we obtain a more accurate estimate of the true gradient by leveraging the gradient dynamics and past estimates, thereby enhancing the performance of DP optimizers. To address the inherent inefficiency of the Kalman filter, we introduce a series of simplifications that reduce memory and computational overhead. Our main contributions can be summarized as follows:

- **Algorithm Design:** We introduce a novel Kalman filter-based approach designed to mitigate DP noise and enhance the performance of various DP optimizers.
- **Algorithm Simplification:** We simplify the Kalman filtering process to significantly reduce memory and computational overhead. This simplified approach, DiSK, requires only one additional forward step and two extra optimizer states.
- **Theoretical Analysis:** We provide theoretical analyses of DiSK, demonstrating that the algorithm is convergent. Moreover, we showed that, compared to DPSGD, DiSK improves the iteration complexity upper-bound by a constant factor.
- **Numerical Results:** Extensive experiments across various models, datasets, and optimizers demonstrate that DiSK significantly boosts DP training performance. Specifically, under the same privacy budgets, DiSK exhibits substantial improvements in test accuracy for training-from-scratch scenarios: a notable increase from 32.4% to 36.9% on the ImageNet-1k dataset, a considerable rise from 63% to 75% on CIFAR-10, and a remarkable improvement from 21% to 42% on CIFAR-100. Furthermore, in fine-tuning tasks, DiSK demonstrates remarkable improvements: an increase from 85% to 89% on CIFAR-100 and an improvement from 81% to 86% on the GLUE dataset. *These results surpass state-of-the-art DP training performance under the same privacy guarantees.*

2 PRELIMINARIES

2.1 PROBLEM DEFINITION & NOTATIONS

Typical training procedures require solving the empirical risk minimization (ERM) problem

$$\min_{\mathbf{x} \in \mathbb{R}^d} \left(F(\mathbf{x}) = \frac{1}{N} \sum_{\xi \in \mathcal{D}} f(\mathbf{x}; \xi) \right), \quad (1)$$

where $\mathbf{x} \in \mathbb{R}^d$ is the optimization variable, $\mathcal{D} = \{\xi_1, \dots, \xi_N\}$ is the training dataset with $|\mathcal{D}| = N$ samples, and $f(\cdot)$ denotes the (possibly non-convex) loss function parameterized by \mathbf{x} and evaluated on sample ξ . For solving the above optimization problem, we rely on iterative procedures, such as SGD, where the parameters are updated over the iterations $t = 1, 2, \dots$. Throughout the paper, we use $(\cdot)_t$ to denote the variables at iteration t , and use \mathbf{I}_d to denote the identity matrix of dimension d .

2.2 DIFFERENTIALLY PRIVATE OPTIMIZATION

Let us start by recalling the definition of (ϵ, δ) -Differential Privacy:

Definition 1 ((ϵ, δ) -DP (Dwork & Roth, 2014)) *A randomized mechanism \mathcal{M} is said to be (ϵ, δ) -differentially private if for any two neighboring datasets $\mathcal{D}, \mathcal{D}'$ ($\mathcal{D}, \mathcal{D}'$ differ only by one sample) and for any measurable output set \mathcal{S} , it holds that $\Pr[\mathcal{M}(\mathcal{D}) \in \mathcal{S}] \leq e^\epsilon \Pr[\mathcal{M}(\mathcal{D}') \in \mathcal{S}] + \delta$.*

A widely used approach to achieving differential privacy (DP) when solving ERM problem (1) is to employ differentially private stochastic gradient descent (Abadi et al., 2016) and its variants, such as DP-Adam and DP-Lora (Yu et al., 2021). To ensure DP, DPSGD leverages the Gaussian mechanism (Dwork & Roth, 2014; Abadi et al., 2016), injecting carefully calibrated Gaussian noise into the gradients at each iteration of the optimization process. This noise injection effectively masks the contribution of individual data points, thereby providing the desired privacy guarantee.

Definition 2 (Gaussian Mechanism (Dwork & Roth, 2014; Balle & Wang, 2018)) *Suppose an algorithm $\mathcal{A} : \mathcal{D} \rightarrow \mathbb{R}^d$ has ℓ_2 sensitivity $\Delta_{\mathcal{A}}$, i.e., $\max_{\mathcal{D}, \mathcal{D}'} \|\mathcal{A}(\mathcal{D}) - \mathcal{A}(\mathcal{D}')\| \leq \Delta_{\mathcal{A}}$. Then, for any $\epsilon > 0$ and $\delta \leq 0.05$, by adding a carefully chosen random Gaussian noise to the output of the algorithm, we can make the algorithm (ϵ, δ) -DP. More specifically, the mechanism $M(x) = \mathcal{A}(x) + \mathbf{w}$, with $\mathbf{w} \sim \mathcal{N}(0, \sigma_{\text{DP}}^2 \mathbf{I}_d)$ and σ_{DP} satisfies $\Phi\left(\frac{\Delta_{\mathcal{A}}}{2\sigma_{\text{DP}}} - \frac{\epsilon\sigma_{\text{DP}}}{\Delta_{\mathcal{A}}}\right) - e^\epsilon \Phi\left(-\frac{\Delta_{\mathcal{A}}}{2\sigma_{\text{DP}}} - \frac{\epsilon\sigma_{\text{DP}}}{\Delta_{\mathcal{A}}}\right) \leq \delta$ is (ϵ, δ) -DP, where $\Phi(t) = \mathbb{P}[\mathcal{N}(0, 1) \leq t]$ is the cumulative density function of normal distribution.*

The DPSGD algorithm, outlined in Algorithm 1, operates by first sampling a mini-batch \mathcal{B}_t of size B and computing the per-sample gradients at each iteration t . To guarantee differential privacy, it then applies the Gaussian mechanism, which involves clipping each per-sample gradient to bound its sensitivity to a maximum value C and subsequently injecting Gaussian noise. The clipping operation $\text{clip}(\nabla f, C) = \min\left\{1, \frac{C}{\|\nabla f\|}\right\} \cdot \nabla f$, often implemented by scaling the gradient when its norm exceeds C , limits the influence of any single data point, while the added noise further masks individual contributions, ensuring the desired privacy level (Abadi et al., 2016).

Theorem 1 (Privacy Guarantee (Abadi et al., 2016)) *Given the number of samples N , the batch-size B , total number of iterations T and clipping threshold C , there exist positive constants u, v , such that for any $\epsilon < \frac{uB^2T}{N^2}$ and $0 < \delta$, by choosing $\sigma_{\text{DP}}^2 \geq v \frac{C^2 T \ln(\frac{1}{\delta})}{N^2 \epsilon^2}$, Algorithm 1 is (ϵ, δ) -DP.*

Theorem 1 implies that the variance of the DP noise injected into the gradients, $\mathbb{E}[\|\mathbf{w}_t\|^2] = d\sigma_{\text{DP}}^2$, scales linearly with both the number of iterations T and the number of parameters d . This presents a significant challenge in modern deep learning, where models size d is large (e.g., 22M-632M for ViT (Dosovitskiy et al., 2020), 137M-1.6B for GPT-2 (Radford et al., 2019)) and require extensive training (e.g., 300K for ViT (Dosovitskiy et al., 2020) and 250K for training Llama (Touvron et al., 2023)). Consequently, the magnitude of the injected DP noise can become substantial, leading to a considerable degradation in model performance.

2.3 KALMAN FILTER

The Kalman filter is a powerful algorithm that provides estimates of unknown variables by iteratively incorporating a series of measurements over time (Welch et al., 1995). To illustrate its application, let us consider a linear dynamic system characterized by the *System update* and *Observation* equations:

$$\begin{aligned} \boldsymbol{\theta}_t &= \mathbf{A}\boldsymbol{\theta}_{t-1} + \mathbf{u}_t + \mathbf{v}_t, & (\text{System update}) \\ \boldsymbol{\psi}_t &= \mathbf{C}\boldsymbol{\theta}_t + \mathbf{w}_t, & (\text{Observation}) \end{aligned} \quad (2)$$

where $\mathbf{A} \in \mathbb{R}^{d_\theta \times d_\theta}$, $\mathbf{C} \in \mathbb{R}^{d_\psi \times d_\theta}$ are the transition and observation matrices; $\boldsymbol{\theta}_t \in \mathbb{R}^{d_\theta}$ is the unknown variable to be tracked/estimated; $\boldsymbol{\psi}_t \in \mathbb{R}^{d_\psi}$ denotes the observation of the system; $\mathbf{u}_t \in \mathbb{R}^{d_\theta}$ denotes the known input; and $\mathbf{v}_t \in \mathbb{R}^{d_\theta}$, $\mathbf{w}_t \in \mathbb{R}^{d_\psi}$ are the process and observation noises that follow Gaussian distribution $\mathcal{N}(0, \Sigma_{\mathbf{v}}), \mathcal{N}(0, \Sigma_{\mathbf{w}})$, respectively. Then, the Kalman filter uses the

following updates to track $\{\theta_t\}$ (Welch et al., 1995):

$$\begin{aligned}
\hat{\theta}_{t|t-1} &= \mathbf{A}\hat{\theta}_{t-1} + \mathbf{u}_t & (\text{Prediction}) \\
\mathbf{P}_{t|t-1} &= \mathbf{A}\mathbf{P}_{t-1}\mathbf{A}^\top + \Sigma_{\mathbf{v}} \\
\mathbf{K}_t &= \mathbf{P}_{t|t-1}\mathbf{C}^\top (\mathbf{C}\mathbf{P}_{t|t-1}\mathbf{C}^\top + \Sigma_{\mathbf{w}})^{-1} \\
\tilde{\theta}_t &= (\mathbf{I}_{d_\theta} - \mathbf{K}_t\mathbf{C})\hat{\theta}_{t|t-1} + \mathbf{K}_t\psi_t & (\text{Correction}) \\
\mathbf{P}_t &= (\mathbf{I}_{d_\theta} - \mathbf{K}_t\mathbf{C})\mathbf{P}_{t|t-1}.
\end{aligned} \tag{3}$$

The filter first *predicts* the state $\hat{\theta}_{t|t-1}$ by the system dynamics, and compute the *filter gain* $\mathbf{K}_t \in \mathbb{R}^{d_\theta \times d_\psi}$ based on the covariance matrix $\mathbf{P}_t \in \mathbb{R}^{d_\theta \times d_\theta}$, and *corrects* the prediction with system observation ψ_t to obtain $\tilde{\theta}_t$. The Kalman filter makes use of both the noisy observation and the prior knowledge of the system dynamics to obtain an accurate estimation of the state θ_t .

In this work, we treat the privatized gradients in the DP optimization as noisy observations of the true underlying gradients. By constructing gradient dynamics using Taylor expansion, we establish a framework for applying the Kalman filter to refine these noisy observations and obtain more accurate gradient estimates. To ensure practical applicability for large-scale models, we simplify the Kalman filter, significantly reducing its memory and computational footprint. These improved gradient estimates ultimately lead to enhanced performance in differentially private optimizers.

2.4 RELATED WORKS

Optimization with filters and controllers: The use of filters and controllers in designing and analyzing optimization algorithms has a rich history. Researchers have leveraged high-pass and low-pass filters to enhance gradient estimation in zeroth-order optimization (Chen et al., 2022), employed PID controllers for both centralized and distributed optimization (Wang et al., 2020b), and analyzed optimizers through the lens of control theory, treating them as dynamic systems (Lessard et al., 2016; Hu & Lessard, 2017; Muehlebach & Jordan, 2019; Mohammadi et al., 2024; Badithela & Seiler, 2019; Cyrus et al., 2018; Scherer et al., 2023; Zhang et al., 2023).

Kalman filter for optimization: The Kalman filter has been utilized in convex optimization for reducing stochastic gradient noise (Bittner & Pronzato, 2004; Vuckovic, 2018). Vuckovic (2018) uses the dynamics of the optimization variable and the gradient to construct the Kalman filter to analyze and improve the performance of momentum methods. Bittner & Pronzato (2004) uses gradient and Hessian as its states to construct the dynamic system for SGD to construct a stopping rule. However, these approaches, with their direct application of the Kalman filter, incur prohibitively high computational and memory costs, ranging from $\mathcal{O}(d^3)$ to $\mathcal{O}(d^6)$, rendering them impractical for training large-scale machine learning models.

Improving DP optimization: Numerous techniques have been proposed to enhance DP optimization by mitigating the impact of DP noise. These include adaptive gradient clipping methods that dynamically adjust clipping thresholds (Andrew et al., 2021; Bu et al., 2024), parameter-efficient training strategies employing adapters, low-rank weights, or quantization (Yu et al., 2021; Luo et al., 2021; Yu et al., 2021), and the design of specialized model architectures less susceptible to noise perturbations (De et al., 2022; Papernot et al., 2021; Wang et al., 2020a). Furthermore, drawing inspiration from signal processing, researchers have explored the use of colored high-frequency DP noise to separate it from the gradient (Koloskova et al., 2023) and the application of low-pass filters to extract the gradient signal from noisy observations (Zhang et al., 2024a).

3 ALGORITHM DESIGN

This section introduces the general Noise Reduction for **D**ifferentially Private Optimizers with Simplified **K**alman Filter (DiSK) framework. This approach leverages the inherent dynamics of the gradient and employs Kalman filtering to obtain denoised estimates of the true gradients from their noisy, privatized counterparts. To enhance its practicality for modern deep learning, Section 3.2 details a simplified version of the Kalman filter updates, designed for memory and computational efficiency.

3.1 GRADIENT DYNAMIC AND KALMAN FILTER

To explain our idea of using the Kalman filter for denoising, let us start by first establishing a dynamic system for the gradients, comprising a “system update” equation and an “observation” equation: The **system update** of the gradient dynamics can be derived by the Taylor expansion and quantifying the change of the gradient at iteration t :

$$\begin{aligned}\nabla F(\mathbf{x}_t) &= \nabla F(\mathbf{x}_{t-1}) + \nabla^2 F(\mathbf{x}_{t-1})^\top (\mathbf{x}_t - \mathbf{x}_{t-1}) + R(\mathbf{x}_t) \\ &= \nabla F(\mathbf{x}_{t-1}) + \mathbf{H}_t(\mathbf{x}_t - \mathbf{x}_{t-1}) + \mathbf{v}_t,\end{aligned}\quad (4)$$

where $\mathbf{H}_t := \nabla^2 F(\mathbf{x}_{t-1}) \in \mathbb{R}^{d \times d}$ and $\mathbf{v}_t = \frac{1}{2} \int_0^1 \nabla^3 F(\mathbf{x}_{t-1})(z\mathbf{x}_t + (1-z)\mathbf{x}_{t-1})^{\otimes 2} dz$ is the remainder and $(\cdot)^{\otimes}$ denotes the tensor vector product. The **observation** of the system is defined as the privatized gradient \mathbf{g}_t , which is a stochastic mapping of the true gradient:

$$\mathbf{g}_t = \frac{1}{B} \sum_{\xi \in \mathcal{B}_t} \text{clip}(\nabla f(\mathbf{x}_t, \xi), C) + \mathbf{w}_t = \mathbf{C}_t \nabla F(\mathbf{x}_t) + \mathbf{w}_t', \quad (5)$$

where \mathbf{w}_t' is the observation noise containing the DP noise and sub-sampling noise. \mathbf{C}_t is the observation matrix. If the clipping operation is inactive and $\mathcal{B} = \mathcal{D}$, i.e., the full batch gradient is used, then $\mathbf{C}_t = \mathbf{I}_d$. Otherwise, \mathbf{C}_t depends on the clipping factor and the mini-batch \mathcal{B} . Combining the system update (4) and the observation (5), we can model the system dynamic of the gradient as:

$$\begin{aligned}\nabla F(\mathbf{x}_t) &= \nabla F(\mathbf{x}_{t-1}) + \mathbf{H}_t(\mathbf{x}_t - \mathbf{x}_{t-1}) + \mathbf{v}_t, & (\text{System update}) \\ \mathbf{g}_t &= \mathbf{C}_t \nabla F(\mathbf{x}_t) + \mathbf{w}_t'. & (\text{Observation})\end{aligned}\quad (6)$$

Let us compare our dynamic system with the general one in (2): In our dynamic system, the gradient $\nabla F(\mathbf{x}_t)$ plays the role of the state $\boldsymbol{\theta}_t$. Other parameters in (2) must change to the followings to obtain our gradient dynamic: $\mathbf{A} = \mathbf{I}_d$, $\mathbf{C} = \mathbf{C}_t$, the input $\mathbf{u}_t = \mathbf{H}_t(\mathbf{x}_t - \mathbf{x}_{t-1})$, and the observation $\boldsymbol{\psi}_t = \mathbf{g}_t$. With the above mapping, we can apply the Kalman filter that combines the **system update** and the **observation** of the gradient to improve the overall estimation quality of the actual gradient beyond only using the observation \mathbf{g}_t . However, there are two key challenges when applying Kalman filter to (6): 1) the input $\mathbf{H}_t(\mathbf{x}_t - \mathbf{x}_{t-1})$ is hard to obtain as computing the Hessian matrix \mathbf{H}_t is challenging for large models, and we can only approximate $\mathbf{H}_t(\mathbf{x}_t - \mathbf{x}_{t-1})$; 2) the observation matrix \mathbf{C}_t is an unknown time-varying random matrix. Due to these differences, the traditional Kalman filter (Welch et al., 1995) cannot be directly applied. Instead, we apply the Kalman filter with noisy input and multiplicative observation noise proposed in Wu et al. (2016) to our system (6), leading to the update rules:

$$\begin{aligned}\tilde{\mathbf{g}}_{t|t-1} &= \tilde{\mathbf{g}}_{t-1} + \tilde{\mathbf{H}}_t(\mathbf{x}_t - \mathbf{x}_{t-1}) & (\text{Prediction}) \\ \mathbf{P}_{t|t-1} &= \mathbf{P}_{t-1} + \Sigma_{\mathbf{H}} + \Sigma_{\mathbf{v}} \\ \mathbf{K}_t &= \mathbf{P}_{t|t-1} \mathbb{E}[\mathbf{C}_t]^\top (\Sigma_{\mathbf{w}} + \mathbb{E}[\mathbf{C}_t] (\Sigma_{\mathbf{C}} \mathbf{S}_t + \mathbf{P}_{t|t-1}) \mathbb{E}[\mathbf{C}_t]^\top - \Sigma_{\mathbf{H}})^{-1} \\ \tilde{\mathbf{g}}_t &= \tilde{\mathbf{g}}_{t|t-1} + \mathbf{K}_t(\mathbf{g}_t - \mathbb{E}[\mathbf{C}_t] \tilde{\mathbf{g}}_{t|t-1}) & (\text{Correction}) \\ \mathbf{P}_t &= (\mathbf{I} - \mathbf{K}_t \mathbb{E}[\mathbf{C}_t]) \mathbf{P}_{t|t-1} \\ \mathbf{S}_t &= \mathbb{E}[\tilde{\mathbf{g}}_t \tilde{\mathbf{g}}_t^\top],\end{aligned}$$

where \mathbf{P}_t denotes the covariance matrix of $\tilde{\mathbf{g}}_t$, $\Sigma_{\mathbf{H}}, \Sigma_{\mathbf{w}}, \Sigma_{\mathbf{C}}, \Sigma_{\mathbf{v}}$ denote the covariance matrices of the random variables $\mathbf{H}_t, \mathbf{w}_t, \mathbf{C}_t, \mathbf{v}_t$, respectively, and $\tilde{\mathbf{H}}_t$ is an instantiation/observation of the unknown Hessian matrix \mathbf{H}_t . The difference between the above Kalman filter and the original Kalman filter (3) is highlighted in magenta color. The variance of the Hessian $\tilde{\mathbf{H}}_t$ plays a role in updating $\mathbf{P}_{t|t-1}$, \mathbf{K}_t , and the expectation $\mathbb{E}[\mathbf{C}_t]$ of the random observation matrix \mathbf{C}_t is used for the updates and its variance $\Sigma_{\mathbf{C}}$ also appears in the update of \mathbf{K}_t . Compared to the noisy gradient \mathbf{g}_t , the output of the Kalman filter $\tilde{\mathbf{g}}_t$ has a smaller variance, resulting in improved performance when used in DP optimizers.

The resulting optimizer with the Kalman filter is given in Algorithm 2. The hyper-parameters of the Kalman filter are the expected observation matrix $\mathbb{E}[\mathbf{C}]$ and the variances of the noises in the system, i.e., $\sigma_{\mathbf{w}}^2, \Sigma_{\mathbf{C}}, \Sigma_{\mathbf{H}}$. Here, we dropped subscript t for \mathbf{C}_t for simplicity in our modeling.

3.2 ALGORITHM SIMPLIFICATION

While Algorithm 2 provides a general framework for applying Kalman filtering to various optimizers, it faces significant challenges in terms of computational and memory demands. Specifically, accurately computing the Hessian matrix (\mathbf{H}) for large models under DP constraints is infeasible, the matrix inversion step introduces a cubic computational complexity ($\mathcal{O}(d^3)$), and storing the covari-

Algorithm 2 Optimizer with Kalman Filter

```

1: Input:  $\mathbf{x}_0, \mathcal{D}, \eta, \mathbb{E}[\mathbf{C}], \sigma_{\mathbf{w}}^2, \Sigma_{\mathbf{C}}, \Sigma_{\mathbf{H}}$ 
2: Initialize:  $\tilde{\mathbf{g}}_{-1} = 0, \mathbf{d}_{-1} = 0, \mathbf{P}_{-1} = \sigma_{\mathbf{w}}^2 \mathbf{I}_d$ 
3: for  $t = 0, \dots, T - 1$  do
4:   Randomly draw minibatch  $\mathcal{B}_t$  from  $\mathcal{D}$ 
5:   Compute privatized gradient  $\mathbf{g}_t = \frac{1}{B} \sum_{\xi \in \mathcal{B}_t} \text{clip}(\nabla f(\mathbf{x}_t; \xi), C) + \mathbf{w}_t$  # Gradient observation
6:    $\tilde{\mathbf{g}}_{t|t-1} = \tilde{\mathbf{g}}_{t-1} + \mathbf{H}_t \mathbf{d}_{t-1}$  # Prediction
7:    $\mathbf{P}_{t|t-1} = \mathbf{P}_{t-1} + \Sigma_{\mathbf{H}}$ 
8:    $\mathbf{K}_t = \mathbf{P}_{t|t-1} \mathbb{E}[\mathbf{C}]^\top (\mathbb{E}[\mathbf{C}] (\mathbf{P}_{t|t-1} + \Sigma_{\mathbf{C}} \tilde{\mathbf{g}}_t \tilde{\mathbf{g}}_t^\top) \mathbb{E}[\mathbf{C}]^\top + \sigma_{\mathbf{w}}^2 \mathbf{I}_d - \Sigma_{\mathbf{H}})^{-1}$  # Compute gain
9:    $\tilde{\mathbf{g}}_t = \tilde{\mathbf{g}}_{t|t-1} + \mathbf{K}_t (\mathbf{g}_t - \mathbb{E}[\mathbf{C}] \tilde{\mathbf{g}}_{t|t-1})$  # Compute denoised private gradient
10:   $\mathbf{x}_{t+1} = \text{OptimizerUpdate}(\mathbf{x}_t, \eta, \tilde{\mathbf{g}}_t)$  # Parameter update
11:   $\mathbf{d}_t = \mathbf{x}_{t+1} - \mathbf{x}_t$  # Record update direction
12:   $\mathbf{P}_t = (\mathbf{I} - \mathbf{K}_t \mathbb{E}[\mathbf{C}]) \mathbf{P}_{t|t-1}$  # Update covariance matrix
13: end for

```

ance matrix (\mathbf{P}_t) at each iteration requires quadratic memory ($\mathcal{O}(d^2)$). To address these limitations and arrive at a practical and memory-efficient algorithm, we propose the following simplifications:

Constant \mathbf{C}_t : We simplify the random matrix \mathbf{C}_t to an identity matrix \mathbf{I}_d , and simply model the randomness in the observation as additive noise only. This simplification is achieved in two steps corresponding to the two sources of randomness in \mathbf{C}_t . First, we remove the impact of clipping in \mathbf{C}_t . This is justified when 1) the clipping threshold C is large enough so that clipping is inactive; or when 2) the clipped gradient $\nabla F_C(\mathbf{x})$ has zero curl, so that our method optimizes $F_C(\mathbf{x})$, where

$$F_C(\mathbf{x}) = \int_0^1 \nabla F_C(z\mathbf{x})^\top \mathbf{x} dz, \quad \nabla F_C(\mathbf{x}) = \frac{1}{N} \sum_{\xi \in \mathcal{D}} \text{clip}(\nabla f(\mathbf{x}; \xi), C). \quad (7)$$

Under this assumption, the minibatch clipped gradient $\frac{1}{B} \sum_{\xi \in \mathcal{B}} \text{clip}(\nabla f(\mathbf{x}, \xi), C)$ is an unbiased estimation of $\nabla F_C(\mathbf{x})$. Thus, $\mathbb{E}[\mathbf{C}_t] = \mathbf{I}_d$. Second, the randomness of sub-sampling in \mathbf{C}_t is removed by assuming that the sub-sampled mini-batch gradient only causes additive noise, i.e., $\frac{1}{B} \sum_{\xi \in \mathcal{B}} \text{clip}(\nabla f(\mathbf{x}, \xi), C) = \nabla F_C(\mathbf{x}) + \mathbf{w}_{\text{SGD}}$, so that $\mathbf{C} = \mathbf{I}_d$ and $\Sigma_{\mathbf{C}} = 0$.

Hessian estimation: We apply the following “trick” to bypass the explicit computation of the Hessian matrix, \mathbf{H}_t . Instead, we approximate the Hessian-vector product, $\mathbf{H}_t(\mathbf{d}_{t-1})$, using a finite difference method (Pearlmutter, 1994):

$$\mathbf{H}_t \mathbf{d}_{t-1} = \frac{\nabla F(\mathbf{x}_t + \gamma \mathbf{d}_{t-1}) - \nabla F(\mathbf{x}_t)}{\gamma} + \mathcal{O}(\gamma) \approx \frac{1}{B} \sum_{\xi \in \mathcal{B}} \frac{\nabla f(\mathbf{x}_t + \gamma \mathbf{d}_{t-1}; \xi) - \nabla f(\mathbf{x}_t; \xi)}{\gamma},$$

This estimation eliminates the need for expensive Hessian computations and significantly reduces both memory and computational complexity.

Simplification of $\Sigma_{\mathbf{H}}$: Few matrix computation steps in Algorithm 2 are extremely time-consuming and memory inefficient. Specifically, the matrix inversion in Line 8 of Algorithm 2 incurs a cubic computational cost ($\mathcal{O}(d^3)$), which becomes prohibitive for large models with billions of parameters. Therefore, we simplify the algorithm by assuming that the covariance matrix in the Kalman filter is a time-invariant diagonal matrix, i.e., $\Sigma_{\mathbf{H}} = \sigma_H^2 \mathbf{I}_d$. Under this assumption, the matrices \mathbf{P}_t and \mathbf{K}_t become $p_t \mathbf{I}_d, k_t \mathbf{I}_d$, for some scalars p_t, k_t . Thus, we reduce all matrix computations to efficient scalar-vector multiplications. Furthermore, the memory complexity for storing these matrices is reduced to $\mathcal{O}(1)$, making our algorithm a viable option for DP training of large-scale models.

Filter gain simplification: With the above simplification, the updates of p_t, k_t simplifies to $p_t = \frac{(\sigma_{\mathbf{w}}^2 - \sigma_H^2)(p_{t-1} + \sigma_{\mathbf{v}}^2 + \sigma_H^2)}{p_{t-1} + \sigma_{\mathbf{v}}^2 + \sigma_{\mathbf{w}}^2}$, $k_t = \frac{p_{t-1} + \sigma_{\mathbf{v}}^2 + \sigma_H^2}{p_{t-1} + \sigma_{\mathbf{v}}^2 + \sigma_{\mathbf{w}}^2}$. Therefore, k_t converges to its stable value with a linear rate, i.e., $\|k_t - k_\infty\| = \mathcal{O}(c_k^t)$, where $c_k = \frac{2\sigma_{\mathbf{w}}^2 + 3\sigma_H^2 + \sigma_{\mathbf{v}}^2 - \sqrt{(\sigma_{\mathbf{v}}^2 + \sigma_H^2)(4\sigma_{\mathbf{w}}^2 + \sigma_{\mathbf{v}}^2 - 3\sigma_H^2)}}{2\sigma_{\mathbf{w}}^2 + 3\sigma_H^2 + \sigma_{\mathbf{v}}^2 + \sqrt{(\sigma_{\mathbf{v}}^2 + \sigma_H^2)(4\sigma_{\mathbf{w}}^2 + \sigma_{\mathbf{v}}^2 - 3\sigma_H^2)}} \in (0, 1)$ (see derivations in Appendix A.3). So we can use constant $k_t = \kappa, \forall t$ to further simplify the algorithm and avoid iteratively updating p_t and recomputing k_t for each step.

With the above simplifications, the complex Algorithm 2 simplifies to DiSK in Algorithm 3. For a detailed walkthrough of this simplification process, please refer to Appendix A.3. This simplified algorithm computes and privatizes the linear combination of the gradient evaluated at two points,

Algorithm 3 DiSK: Differentially private optimizer with Simplified Kalman filter

```

1: Input:  $\mathbf{x}_0, \mathcal{D}, \eta, \gamma, \kappa, C, \sigma_{\text{DP}}$ 
2: Initialize:  $\tilde{\mathbf{g}}_{-1} = \mathbf{g}_0, \mathbf{d}_{-1} = 0$ 
3: for  $t = 0, \dots, T - 1$  do
4:   Randomly draw minibatch  $\mathcal{B}_t$  from  $\mathcal{D}$ 
5:   Compute  $\mathbf{g}_t = \frac{1}{B} \sum_{\xi \in \mathcal{B}_t} \text{clip} \left( \frac{1-\kappa}{\kappa\gamma} \nabla f(\mathbf{x}_t + \gamma \mathbf{d}_{t-1}; \xi) + (1 - \frac{1-\kappa}{\kappa\gamma}) \nabla f(\mathbf{x}_t; \xi), C \right) + \mathbf{w}_t$ 
        where  $\mathbf{w}_t \sim \mathcal{N}(0, \sigma_{\text{DP}}^2 \cdot \mathbf{I}_d)$ 
6:    $\tilde{\mathbf{g}}_t = (1 - \kappa) \tilde{\mathbf{g}}_{t-1} + \kappa \mathbf{g}_t$  # Apply filter
7:    $\mathbf{x}_{t+1} = \text{OptimizerUpdate}(\mathbf{x}_t, \eta, \tilde{\mathbf{g}}_t)$  # Parameter update
8:    $\mathbf{d}_t = \mathbf{x}_{t+1} - \mathbf{x}_t$  # Record update direction
9: end for

```

$\mathbf{x}_t, \mathbf{x}_t + \gamma \mathbf{d}_t$. Then, this privatized combination undergoes exponential weighted averaging to obtain $\tilde{\mathbf{g}}_t$, which serves as the input to the base optimizer (Line 7 of Algorithm 3).

3.3 ADDITIONAL DISCUSSION

Memory and computation cost: Algorithm 3 requires one additional forward step to compute $f(\mathbf{x}_t + \gamma \mathbf{d}_{t-1}; \xi)$. This means that the algorithm has at most twice the computational cost of the baseline DP-SGD algorithm. Moreover, Algorithm 3 only requires two additional states to store: $\tilde{\mathbf{g}}_t$ and \mathbf{d}_t . Compared to DPSGD, which requires storing the model and the gradient, DiSK has at most twice the memory cost; and compared to DPAdam, which requires storing the first- and second-order moments, the algorithm has at most $1.5\times$ the memory cost.

Connection to NAG and STORM: Remarkably, Algorithm 3 has an implicit connection to the (unified) Nesterov accelerated gradient (NAG) method (Shen et al., 2023; Sutskever et al., 2013) and the Stochastic Recursive Momentum (STORM) algorithm (Cutkosky & Orabona, 2019). Specifically, by letting the OptimizerUpdate be SGD, assuming clipping is inactive, and setting $\mathbf{w}_t = 0$ (i.e., without privatizing the gradient) in Algorithm 3, we can make a clear connection: On one hand, DiSK reduces to NAG by choosing $\gamma = \frac{1-\kappa}{\kappa}, \eta = \kappa, 1 - \kappa = \mu$, and $B = N$. On the other hand, the update of DiSK matches STORM by choosing $\gamma = -1, \kappa = \alpha$, and $B = 1$. A detailed derivation and discussion is provided in Appendix A.4. This observation reveals an intriguing connection between NAG (designed for acceleration) and STORM (focused on variance reduction), unifying them within the framework of DiSK, a Kalman filtering-based algorithm.

Connection to DOPPLER: DOPPLER (Zhang et al., 2024a) and DiSK both use a filter to separate the gradient signal from the DP noise. If \mathbf{g}_t only evaluates the gradient at one point instead of using the linear combination of gradients at two points in Algorithm 3, Line 5, DiSK becomes DOPPLER with a first-order filter. The key difference is that DOPPLER assumes an underlying low-frequency dynamic of the gradient and applies a time-invariant low-pass filter. Designing the optimal low-pass filter relies on the prior knowledge of the gradient frequency spectrum, which is hard to obtain in practice, and implementing such a high-order low-pass filter results in a large memory overhead. While in DiSK, we do not assume the frequency property of the gradient signal. Instead, we incorporate the gradient dynamics into the filtering procedure and use the Kalman filter, a predictive filtering approach, to reduce the impact of DP noise.

4 THEORETICAL ANALYSIS

This section includes theoretical analyses of Algorithm 3. Our study establishes the convergence, provable noise reduction, and the privacy-utility trade-off of the algorithm. To facilitate our analysis, we make the following assumptions:

A 1 (Smoothness) $f(\cdot, \xi)$ is L -smooth for any ξ , i.e., $\|\nabla f(\mathbf{x}; \xi) - \nabla f(\mathbf{y}; \xi)\| \leq L \|\mathbf{x} - \mathbf{y}\|$, $\forall \xi \in \mathcal{D}, \forall \mathbf{x}, \mathbf{y} \in \mathbb{R}^d$.

A 2 (Bounded Variance) The per-sample gradient has bounded variance with $\mathbb{E}_{\xi \in \mathcal{D}} \|\nabla f(\mathbf{x}; \xi) - \nabla F(\mathbf{x})\|^2 \leq \sigma_{\text{SGD}}^2$, $\forall \mathbf{x} \in \mathbb{R}^d$, where $\mathbb{E}_{\xi \in \mathcal{D}}[\cdot]$ denotes the expectation taken on the randomness over ξ that is uniformly sampled from dataset \mathcal{D} .

A 3 (Bounded Gradient) Each per-sample gradient has a bounded norm, i.e., $\|\nabla f(\mathbf{x}; \xi)\| \leq G$, $\forall \mathbf{x} \in \mathbb{R}^d, \forall \xi \in \mathcal{D}$.

Let us briefly comment on these assumptions: A1 and A2 are standard in non-convex optimization (Allen-Zhu & Hazan, 2016; Zaheer et al., 2018; Abadi et al., 2016); and A3 is commonly used in analyzing the convergence of DP algorithms (Abadi et al., 2016; Wang et al., 2020a; Andrew et al., 2021) to avoid introducing the clipping bias. Since the impact of clipping is not the major focus of this paper, we follow this tradition and use A3 to simplify our theoretical analysis.

4.1 CONVERGENCE ANALYSIS

We provide the following convergence results for Algorithm 3, assuming σ_{DP} being a constant.

Theorem 2 Assume A1-A3 hold. Fix σ_{DP}^2 and choose $C \geq (1 + \frac{2(1-\kappa)}{\kappa})G$, κ, η satisfy

$$\eta < \frac{1 + \kappa}{2L(1 + 2(1 - \kappa)^2\beta L(2 + |1 + \gamma|C_\gamma))}, \quad \kappa > 1 - \frac{1}{\sqrt{1 + 4\eta^2L^2 + |1 + \gamma|(\kappa + 2\eta^2L^2C_\gamma)}},$$

and run Algorithm 3 for T iterations. Then,

$$\begin{aligned} \frac{1}{T} \sum_{t=0}^T \mathbb{E} \|\nabla F(\mathbf{x}_t)\|^2 &\leq \frac{2(F(\mathbf{x}_0) + \beta \|\nabla F(\mathbf{x}_0)\|^2 - F^*)}{C_1\eta T} \\ &\quad + \frac{2(\beta + \eta^2L)\kappa^2}{C_1\eta} \left(\frac{(2 + |1 + \gamma|)\sigma_{\text{SGD}}^2}{B} + d\sigma_{\text{DP}}^2 \right), \end{aligned} \quad (8)$$

where $C_\gamma = 1 + \frac{4(2+1/\kappa+|1+\gamma|)}{\gamma^2}$, $C_1 = (1+\kappa-2\eta L) - 4(\beta+\eta^2L)(1-\kappa)^2L^2\eta(2+|1+\gamma|C_\gamma) > 0$, and $\beta \geq \frac{\eta(1-\kappa)/2 + \eta^2L(1-\kappa)^2(1+4\eta^2L^2+|1+\gamma|(\kappa+2\eta^2L^2C_\gamma))}{1-(1-\kappa)^2(1+4\eta^2L^2+|1+\gamma|(\kappa+2\eta^2L^2C_\gamma))} \geq 0$ are some non-negative constants.

The proof of Theorem 2 is relegated to Appendix B. Notice that when $\kappa = 1$, we have $\beta = 0$, $C_1 = 2(1 - \eta L)$ and the convergence result recovers that of DPSGD (Ghadimi & Lan, 2013; Zhang et al., 2017). With this theorem, we can choose specific parameters and obtain the following corollary:

Corollary 1 Under the conditions of Theorem 2, choose $\gamma = -1$,

$$\begin{aligned} \eta &= \min \left\{ \frac{1}{L(2 + 4/C_\kappa - C_\kappa)}, \frac{1}{C_\kappa L} \sqrt{\frac{2C_\kappa L(F(\mathbf{x}_0) - F^*) + \|\nabla F(\mathbf{x}_0)\|^2}{T(2\sigma_{\text{SGD}}^2/B + d\sigma_{\text{DP}}^2)}} \right\}, \\ \beta &= \frac{\eta(1 - \kappa)/2 + \eta^2L(1 - \kappa)^2(1 + 4\eta^2L^2)}{1 - (1 - \kappa)^2(1 + 4\eta^2L^2)} \leq \frac{1}{2C_\kappa L}, \\ \kappa &= C_\kappa L\eta \leq 1, \quad \text{and} \quad C_\kappa = \min \left\{ \frac{\|\nabla F(\mathbf{x}_0)\|^2}{2L(F(\mathbf{x}_0) - F^*)}, 1 \right\}, \end{aligned}$$

then Algorithm 3 satisfies:

$$\frac{1}{T} \sum_{t=0}^T \mathbb{E} [\|\nabla F(\mathbf{x}_t)\|^2] \leq 4 \sqrt{\frac{C_\kappa L(F(\mathbf{x}_0) - F^*)(2\sigma_{\text{SGD}}^2/B + d\sigma_{\text{DP}}^2)}{T}} = \mathcal{O} \left(\sqrt{\frac{d}{T}} \right). \quad (9)$$

Convergence improvement: The above result implies that the *order* of the number of iterations T needed for convergence of Algorithm 3 is the same as of DPSGD (Ghadimi & Lan, 2013; Zhang et al., 2017). However, Algorithm 3 has a *constant factor* improvement in its convergence rate over DPSGD. This improvement is resulted from the presence of $C_\kappa \leq 1$ in the numerator in the RHS of (9). More specifically, if $C_\kappa < 1$, i.e., $\|\nabla F(\mathbf{x}_0)\|^2 < 2L(F(\mathbf{x}_0) - F^*)$, then the convergence bound reduces by a factor of $\sqrt{1/C_\kappa}$, and DiSK has clear theoretical improvement over vanilla DPSGD. **Case I:** For (μ -strongly) convex problems, it is guaranteed that $2\mu(F(\mathbf{x}_0) - F^*) \leq \|\nabla F(\mathbf{x}_0)\|^2 \leq 2L(F(\mathbf{x}_0) - F^*)$. Therefore, the factor $C_\kappa \in [\mu/L, 1]$. **Case II:** When training highly non-convex deep learning models, the Lipschitz constant L can be large (Herrera et al., 2020), and $2L(F(\mathbf{x}_0) - F^*)$ can be much larger than $\|\nabla F(\mathbf{x}_0)\|^2$, which results in a considerable algorithm performance improvement compared to vanilla DPSGD.

While the above corollary is for the case of $\gamma = -1$, we can obtain performance improvement for $\gamma \neq -1$ as well. The choice $\gamma = -1$ is optimized for the *worst case* (function satisfying our assumptions) based on our upper-bound in (8). However, it is possible that for functions satisfying additional assumptions, other choices of γ lead to better convergence result. This fact is further explained after presenting the proof of the theorem in Appendix B.2.

As a last remark in this subsection, notice that our iteration complexity improvement does not require any additional assumption on the problem. In contrast, existing works with convergence improvement require additional assumptions, e.g., on the correlation between the gradients (Zhang et al., 2024a), or on the trace of Hessian (Choquette-Choo et al., 2024; Li et al., 2022).

4.2 PRIVACY-UTILITY TRADE-OFF

To provide DP, the Subsampled Gaussian mechanism is used in Lines 4 and 5 of Algorithm 3. Instead of $\nabla f(\mathbf{x}_t; \xi)$, we treat $\frac{1-\kappa}{\kappa\gamma} \nabla f(\mathbf{x}_t - \gamma \mathbf{d}_{t-1}; \xi) + (1 - \frac{1-\kappa}{\kappa\gamma}) \nabla f(\mathbf{x}_t; \xi)$ as the per-sample gradient and apply the Subsampled Gaussian mechanism to privatize it. Therefore, Algorithm 3 and DPSGD share a similar privacy guarantee, as the privacy proof directly follows the Subsampled Gaussian mechanism and the composition of T iterations in Theorem 1. Specifically, by combining Theorem 1 and Theorem 2, we obtain the following privacy-utility trade-off:

Theorem 3 Assume A1-A3 holds. Run Algorithm 3 for $T = \frac{\sqrt{2}N\epsilon\sigma_{\text{SGD}}}{C\sqrt{Bd\ln(1/\delta)}}$ iterations, and choose κ, β according to the choices in Corollary 1, then

$$\frac{1}{T} \sum_{t=0}^T \mathbb{E} \|\nabla F(\mathbf{x}_t)\|^2 \leq \frac{8C\sigma_{\text{SGD}} \sqrt{C_\kappa L(F(\mathbf{x}_0) - F^*)d\ln(1/\delta)}}{\sqrt{BN}\epsilon} = \mathcal{O}\left(\frac{\sqrt{d\ln(1/\delta)}}{N\epsilon}\right) \quad (10)$$

Similar to our convergence result, compared to vanilla DPSGD, the privacy-utility trade-off of Algorithm 3 reduces by a constant factor of $\sqrt{1/C_\kappa}$. To the best of our knowledge, this is the first theoretical result on the utility improvement of a DPSGD-type algorithm without any additional assumptions on the problem.

5 NUMERICAL EXPERIMENTS

We perform extensive pre-training and fine-tuning experiments on various image classification (CV) and natural language processing (NLP) tasks using different base algorithms, privacy budgets, and models. The implementation details of the experiments are given in Appendix C.1. The link to the code is <https://anonymous.4open.science/r/KalmanDP-BEDB>.

5.1 EXPERIMENT SETTINGS

Dataset: We train the models on one synthetic dataset, four CV datasets, including MNIST (Deng, 2012), CIFAR-10/CIFAR-100 (Krizhevsky et al., 2009), and ImageNet-1k (Deng et al., 2009), and three NLP dataset, including GLUE (Wang et al., 2018), E2E (Novikova et al., 2017), and DART (Nan et al., 2021).

Model: For the CV tasks, we use three different models, including a 5-layer CNN, WideResNet (WRN) (De et al., 2022), and ViT (Dosovitskiy et al., 2020), representing three typical CV model structures. For the NLP task, we use the RoBERTa (Liu et al., 2019) and the GPT-2 (Radford et al., 2019) models. For pre-training, the models are initialized with random weights, and for fine-tuning with ViT, RoBERTa, and GPT-2, we directly use the checkpoints on HuggingFace (Wolf et al., 2020).

Algorithm: We use the DP version of SGD and Adam for CV tasks, and AdamW for NLP tasks as baselines. Then, we apply DiSK to compare their performance. Additional results on LoRA (Li et al., 2021) are given in Appendix C.4. In the results, we use **KF-** to denote the privatized version of the algorithms with the DiSK framework.

Hyper-parameter choices: We tune the hyper-parameters using a grid search. Specifically, we conduct a grid search on the batch size B , total epochs $E = NT/B$, and step size η for each given privacy budget ϵ . For all experiments, we fix the privacy parameter $\delta = 1/N^{1.1}$ to obtain a reasonable privacy notion. Detailed hyper-parameter choices are discussed in Appendix C.2.

5.2 NUMERICAL RESULTS

CV tasks: We first train the CV models with randomly initialized weights on different image datasets. The results for 5-layer CNN on the MNIST dataset, 5-layer CNN on the CIFAR-10 dataset,

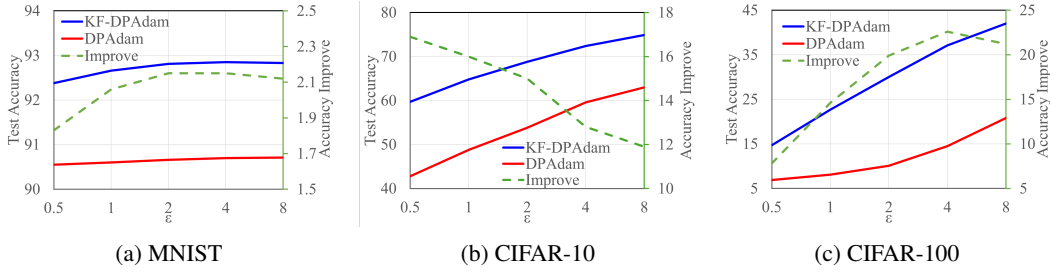


Figure 1: Test accuracy of training from scratch on MNIST, CIFAR-10, and CIFAR-100 datasets with and without DiSK for different privacy budgets.

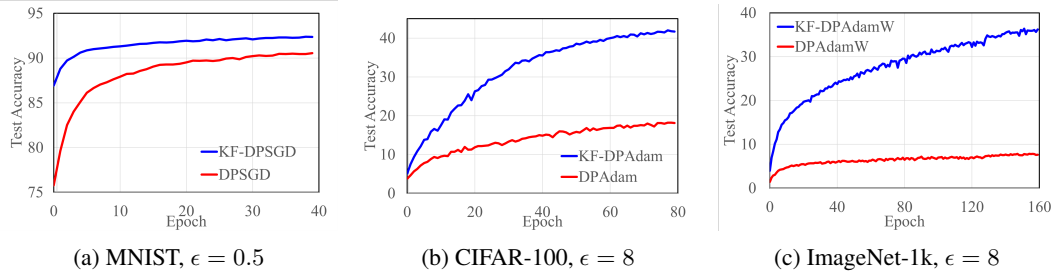


Figure 2: Test accuracy on MNIST, CIFAR-100, and validation accuracy on ImageNet-1k datasets training from scratch with and without DiSK for fixed privacy budgets.

Table 1: Test accuracy of fine-tuning result on the GLUE dataset.

Task	$(\epsilon = \infty)$	$\epsilon = 6.7$			$\epsilon = 1$		
	Non-DP	DP	KF-DP	KF-DPLora	DP	KF-DP	KF-DPLora
MNLI	87.6	83.2	84.8	85.9	80.7	82.0	84.7
QNLI	92.8	87.5	88.9	90.5	86.0	88.7	90.3
SST-2	94.8	91.5	92.8	93.1	91.4	91.5	92.9
QQP	91.9	85.8	88.5	89.0	84.2	86.9	87.8

and WRN-16-4 on the CIFAR-100 datasets with different privacy budgets are given in Figure 1. DiSK significantly outperforms the base algorithm across all used privacy budgets.

The test accuracy curves during the training for 5-layer CNN on the MNIST dataset, WRN-16-4 on the CIFAR-100 dataset, and ViT-small on the ImageNet-1k dataset are given in Figure 2. The optimizer with DiSK converges faster than the base algorithm on all tasks and reaches a higher final accuracy at a given privacy budget. The test accuracy of CIFAR-100 achieves 41.8%, and ImageNet-1k achieves 36.4%, which outperforms the SOTA results that apply data augmentation under the same privacy budget (40.6% for CIFAR-100 (Bao et al., 2024) and 32.4% for ImageNet-1k (De et al., 2022)). Additional comparisons on different models, algorithms, and fine-tuning CIFAR-100 are given in Appendix C.3.

NLP tasks: We fine-tune a pre-trained RoBERTa-base model¹ on the GLUE datasets. The final test accuracy for is given in Table 1. We follow the same training script and hyper-parameter choices in the experiments as Bu et al. (2024). Compared with the base algorithm (DPAdamW), DiSK improves the final accuracy on all tasks by at least 3.8% when $\epsilon = 1$ and 1.3% when $\epsilon = 6.7$. Additional results for text generation tasks on the E2E and DART datasets are given in Appendix C.4.

Ablation study: We conduct ablation studies on the choice of the hyper-parameters of DiSK, specifically, how κ, γ impact the algorithm performance. The results are presented in Appendix C.3.

Improvements over the SOTA: Table 6 in Appendix C.5 summarizes the improvements of DiSK over the SOTA on different tasks.

¹<https://huggingface.co/FacebookAI/roberta-base>

REPRODUCIBILITY STATEMENT

For the algorithm implementation, we provide a link to an anonymous downloadable source code in Section 5. We also discussed the data, model, and algorithms used in the experiment in Section 5 and in Appendix C. For our theoretical results provided in Section 4, we also include clear explanations of the assumptions in the section. The complete proof of the theorems can be found in Appendix B.

BROADER IMPACT

This paper presents work that aims to advance the field of Machine Learning, combining optimization with signal processing and control societies. There are many potential societal consequences of our work, none of which we feel must be specifically highlighted here.

REFERENCES

- Martin Abadi, Andy Chu, Ian Goodfellow, H Brendan McMahan, Ilya Mironov, Kunal Talwar, and Li Zhang. Deep learning with differential privacy. In *Proceedings of the 2016 ACM SIGSAC conference on computer and communications security*, pp. 308–318, 2016.
- Zeyuan Allen-Zhu and Elad Hazan. Variance reduction for faster non-convex optimization. In *International conference on machine learning*, pp. 699–707. PMLR, 2016.
- Galen Andrew, Om Thakkar, Brendan McMahan, and Swaroop Ramaswamy. Differentially private learning with adaptive clipping. *Advances in Neural Information Processing Systems*, 34:17455–17466, 2021.
- Apurva Badithela and Peter Seiler. Analysis of the heavy-ball algorithm using integral quadratic constraints. In *2019 American control conference (ACC)*, pp. 4081–4085. IEEE, 2019.
- Borja Balle and Yu-Xiang Wang. Improving the gaussian mechanism for differential privacy: Analytical calibration and optimal denoising. In *International Conference on Machine Learning*, pp. 394–403. PMLR, 2018.
- Wenxuan Bao, Francesco Pittaluga, Vijay Kumar BG, and Vincent Bindschaedler. Dp-mix: mixup-based data augmentation for differentially private learning. *Advances in Neural Information Processing Systems*, 36, 2024.
- Barbara Bittner and Luc Pronzato. Kalman filtering in stochastic gradient algorithms: construction of a stopping rule. In *2004 IEEE International Conference on Acoustics, Speech, and Signal Processing*, volume 2, pp. ii–709. IEEE, 2004.
- Zhiqi Bu, Yu-Xiang Wang, Sheng Zha, and George Karypis. Differentially private optimization on large model at small cost. In *International Conference on Machine Learning*, pp. 3192–3218. PMLR, 2023.
- Zhiqi Bu, Yu-Xiang Wang, Sheng Zha, and George Karypis. Automatic clipping: Differentially private deep learning made easier and stronger. *Advances in Neural Information Processing Systems*, 36, 2024.
- Xin Chen, Yujie Tang, and Na Li. Improve single-point zeroth-order optimization using high-pass and low-pass filters. In *International Conference on Machine Learning*, pp. 3603–3620. PMLR, 2022.
- Christopher A Choquette-Choo, Krishnamurthy Dj Dvijotham, Krishna Pillutla, Arun Ganesh, Thomas Steinke, and Abhradeep Guha Thakurta. Correlated noise provably beats independent noise for differentially private learning. In *The Twelfth International Conference on Learning Representations*, 2024.
- Ashok Cutkosky and Francesco Orabona. Momentum-based variance reduction in non-convex sgd. *Advances in neural information processing systems*, 32, 2019.

- Saman Cyrus, Bin Hu, Bryan Van Scoy, and Laurent Lessard. A robust accelerated optimization algorithm for strongly convex functions. In *2018 Annual American Control Conference (ACC)*, pp. 1376–1381. IEEE, 2018.
- Soham De, Leonard Berrada, Jamie Hayes, Samuel L Smith, and Borja Balle. Unlocking high-accuracy differentially private image classification through scale. *arXiv preprint arXiv:2204.13650*, 2022.
- Jia Deng, Wei Dong, Richard Socher, Li-Jia Li, Kai Li, and Li Fei-Fei. Imagenet: A large-scale hierarchical image database. In *2009 IEEE conference on computer vision and pattern recognition*, pp. 248–255. Ieee, 2009.
- Li Deng. The mnist database of handwritten digit images for machine learning research [best of the web]. *IEEE signal processing magazine*, 29(6):141–142, 2012.
- Alexey Dosovitskiy, Lucas Beyer, Alexander Kolesnikov, Dirk Weissenborn, Xiaohua Zhai, Thomas Unterthiner, Mostafa Dehghani, Matthias Minderer, Georg Heigold, Sylvain Gelly, et al. An image is worth 16x16 words: Transformers for image recognition at scale. In *International Conference on Learning Representations*, 2020.
- Cynthia Dwork and Aaron Roth. The algorithmic foundations of differential privacy. *Theoretical Computer Science*, 9(3-4):211–407, 2014.
- Saeed Ghadimi and Guanghui Lan. Stochastic first-and zeroth-order methods for nonconvex stochastic programming. *SIAM journal on optimization*, 23(4):2341–2368, 2013.
- Calypso Herrera, Florian Krach, and Josef Teichmann. Estimating full lipschitz constants of deep neural networks. *arXiv preprint arXiv:2004.13135*, 2020.
- Bin Hu and Laurent Lessard. Dissipativity theory for nesterov’s accelerated method. In *International Conference on Machine Learning*, pp. 1549–1557. PMLR, 2017.
- Yuhang Hu, Zhou Tan, Xianxian Li, Jinyan Wang, et al. Adaptive clipping bound of deep learning with differential privacy. In *2021 IEEE 20th International Conference on Trust, Security and Privacy in Computing and Communications (TrustCom)*, pp. 428–435. IEEE, 2021.
- Bargav Jayaraman and David Evans. Evaluating differentially private machine learning in practice. In *28th USENIX Security Symposium (USENIX Security 19)*, pp. 1895–1912, 2019.
- Peter Kairouz, Brendan McMahan, Shuang Song, Om Thakkar, Abhradeep Thakurta, and Zheng Xu. Practical and private (deep) learning without sampling or shuffling. In *International Conference on Machine Learning*, pp. 5213–5225. PMLR, 2021.
- R. E. Kalman. A New Approach to Linear Filtering and Prediction Problems. *Journal of Basic Engineering*, 82(1):35–45, 03 1960. ISSN 0021-9223. doi: 10.1115/1.3662552. URL <https://doi.org/10.1115/1.3662552>.
- Anastasiia Koloskova, Ryan McKenna, Zachary Charles, John Rush, and H Brendan McMahan. Gradient descent with linearly correlated noise: Theory and applications to differential privacy. *Advances in Neural Information Processing Systems*, 36, 2023.
- Alex Krizhevsky, Geoffrey Hinton, et al. Learning multiple layers of features from tiny images. 2009.
- Laurent Lessard, Benjamin Recht, and Andrew Packard. Analysis and design of optimization algorithms via integral quadratic constraints. *SIAM Journal on Optimization*, 26(1):57–95, 2016.
- Xuechen Li, Florian Tramer, Percy Liang, and Tatsunori Hashimoto. Large language models can be strong differentially private learners. In *International Conference on Learning Representations*, 2021.
- Xuechen Li, Daogao Liu, Tatsunori B Hashimoto, Huseyin A Inan, Janardhan Kulkarni, Yin-Tat Lee, and Abhradeep Guha Thakurta. When does differentially private learning not suffer in high dimensions? *Advances in Neural Information Processing Systems*, 35:28616–28630, 2022.

- Guanbiao Lin, Hongyang Yan, Guang Kou, Teng Huang, Shiyu Peng, Yingying Zhang, and Changyu Dong. Understanding adaptive gradient clipping in dp-sgd, empirically. *International Journal of Intelligent Systems*, 37(11):9674–9700, 2022.
- Yinhan Liu, Myle Ott, Naman Goyal, Jingfei Du, Mandar Joshi, Danqi Chen, Omer Levy, Mike Lewis, Luke Zettlemoyer, and Veselin Stoyanov. Roberta: A robustly optimized bert pretraining approach. *arXiv preprint arXiv:1907.11692*, 2019.
- Yuanyuan Liu, Jiacheng Geng, Fanhua Shang, Weixin An, Hongying Liu, Qi Zhu, and Wei Feng. Laplacian smoothing stochastic admm with differential privacy guarantees. *IEEE Transactions on Information Forensics and Security*, 17:1814–1826, 2022.
- Ilya Loshchilov and Frank Hutter. Sgdr: Stochastic gradient descent with warm restarts. In *International Conference on Learning Representations*, 2022.
- Zelun Luo, Daniel J Wu, Ehsan Adeli, and Li Fei-Fei. Scalable differential privacy with sparse network finetuning. In *Proceedings of the IEEE/CVF Conference on Computer Vision and Pattern Recognition*, pp. 5059–5068, 2021.
- H Brendan McMahan, Daniel Ramage, Kunal Talwar, and Li Zhang. Learning differentially private recurrent language models. In *International Conference on Learning Representations*, 2018.
- Harsh Mehta, Abhradeep Guha Thakurta, Alexey Kurakin, and Ashok Cutkosky. Towards large scale transfer learning for differentially private image classification. *Transactions on Machine Learning Research*, 2023.
- Hesameddin Mohammadi, Meisam Razaviyayn, and Mihailo R Jovanović. Tradeoffs between convergence rate and noise amplification for momentum-based accelerated optimization algorithms. *IEEE Transactions on Automatic Control*, 2024.
- Michael Muehlebach and Michael Jordan. A dynamical systems perspective on nesterov acceleration. In *International Conference on Machine Learning*, pp. 4656–4662. PMLR, 2019.
- Linyong Nan, Dragomir Radev, Rui Zhang, Amrit Rau, Abhinand Sivaprasad, Chiachun Hsieh, Xiangru Tang, Aadit Vyas, Neha Verma, Pranav Krishna, Yangxiaokang Liu, Nadia Irwanto, Jessica Pan, Faiaz Rahman, Ahmad Zaidi, Mutethia Mutuma, Yasin Tarabar, Ankit Gupta, Tao Yu, Yi Chern Tan, Xi Victoria Lin, Caiming Xiong, Richard Socher, and Nazneen Fatema Rajani. DART: Open-domain structured data record to text generation. In *Proceedings of the 2021 Conference of the North American Chapter of the Association for Computational Linguistics: Human Language Technologies*, pp. 432–447, Online, June 2021. Association for Computational Linguistics. doi: 10.18653/v1/2021.naacl-main.37. URL <https://aclanthology.org/2021.naacl-main.37>.
- Jekaterina Novikova, Ondrej Dušek, and Verena Rieser. The E2E dataset: New challenges for end-to-end generation. In *Proceedings of the 18th Annual Meeting of the Special Interest Group on Discourse and Dialogue*, Saarbrücken, Germany, 2017. URL <https://arxiv.org/abs/1706.09254>. arXiv:1706.09254.
- Nicolas Papernot, Abhradeep Thakurta, Shuang Song, Steve Chien, and Úlfar Erlingsson. Tempered sigmoid activations for deep learning with differential privacy. In *Proceedings of the AAAI Conference on Artificial Intelligence*, volume 35, pp. 9312–9321, 2021.
- Jinseong Park, Hoki Kim, Yujin Choi, and Jaewook Lee. Differentially private sharpness-aware training. In *International Conference on Machine Learning*, pp. 27204–27224. PMLR, 2023.
- Barak A Pearlmutter. Fast exact multiplication by the hessian. *Neural computation*, 6(1):147–160, 1994.
- Alec Radford, Jeff Wu, Rewon Child, David Luan, Dario Amodei, and Ilya Sutskever. Language models are unsupervised multitask learners. 2019.
- Maria Isabel Ribeiro. Kalman and extended kalman filters: Concept, derivation and properties. *Institute for Systems and Robotics*, 43(46):3736–3741, 2004.

- Carsten W Scherer, Christian Ebenbauer, and Tobias Holicki. Optimization algorithm synthesis based on integral quadratic constraints: A tutorial. In *2023 62nd IEEE Conference on Decision and Control (CDC)*, pp. 2995–3002. IEEE, 2023.
- Li Shen, Congliang Chen, Fangyu Zou, Zequn Jie, Ju Sun, and Wei Liu. A unified analysis of adagrad with weighted aggregation and momentum acceleration. *IEEE Transactions on Neural Networks and Learning Systems*, 2023.
- Ilya Sutskever, James Martens, George Dahl, and Geoffrey Hinton. On the importance of initialization and momentum in deep learning. In *International conference on machine learning*, pp. 1139–1147. PMLR, 2013.
- Qiaoyue Tang, Frederick Shpilevskiy, and Mathias Lécuyer. Dp-adambc: Your dp-adam is actually dp-sgd (unless you apply bias correction). In *Proceedings of the AAAI Conference on Artificial Intelligence*, volume 38, pp. 15276–15283, 2024.
- Hugo Touvron, Thibaut Lavril, Gautier Izacard, Xavier Martinet, Marie-Anne Lachaux, Timothée Lacroix, Baptiste Rozière, Naman Goyal, Eric Hambro, Faisal Azhar, et al. Llama: Open and efficient foundation language models. *arXiv preprint arXiv:2302.13971*, 2023.
- Florian Tramer and Dan Boneh. Differentially private learning needs better features (or much more data). *arXiv preprint arXiv:2011.11660*, 2020.
- James Vuckovic. Kalman gradient descent: Adaptive variance reduction in stochastic optimization. *arXiv preprint arXiv:1810.12273*, 2018.
- Eric A Wan and Rudolph Van Der Merwe. The unscented kalman filter. *Kalman filtering and neural networks*, pp. 221–280, 2001.
- Alex Wang, Amanpreet Singh, Julian Michael, Felix Hill, Omer Levy, and Samuel Bowman. Glue: A multi-task benchmark and analysis platform for natural language understanding. In *Proceedings of the 2018 EMNLP Workshop BlackboxNLP: Analyzing and Interpreting Neural Networks for NLP*, pp. 353–355, 2018.
- Bao Wang, Quanquan Gu, March Boedihardjo, Lingxiao Wang, Farzin Barekat, and Stanley J Osher. Dp-lssgd: A stochastic optimization method to lift the utility in privacy-preserving erm. In *Mathematical and Scientific Machine Learning*, pp. 328–351. PMLR, 2020a.
- Haoqian Wang, Yi Luo, Wangpeng An, Qingyun Sun, Jun Xu, and Lei Zhang. Pid controller-based stochastic optimization acceleration for deep neural networks. *IEEE transactions on neural networks and learning systems*, 31(12):5079–5091, 2020b.
- Wenxiao Wang, Tianhao Wang, Lun Wang, Nanqing Luo, Pan Zhou, Dawn Song, and Ruoxi Jia. Dplis: Boosting utility of differentially private deep learning via randomized smoothing. *Proceedings on Privacy Enhancing Technologies*, 4:163–183, 2021.
- Greg Welch, Gary Bishop, et al. *An introduction to the Kalman filter*. Chapel Hill, NC, USA, 1995.
- Thomas Wolf, Lysandre Debut, Victor Sanh, Julien Chaumond, Clement Delangue, Anthony Moi, Pierric Cistac, Tim Rault, Rémi Louf, Morgan Funtowicz, Joe Davison, Sam Shleifer, Patrick von Platen, Clara Ma, Yacine Jernite, Julien Plu, Canwen Xu, Teven Le Scao, Sylvain Gugger, Mariama Drame, Quentin Lhoest, and Alexander M. Rush. Transformers: State-of-the-art natural language processing. In *Proceedings of the 2020 Conference on Empirical Methods in Natural Language Processing: System Demonstrations*, pp. 38–45, Online, October 2020. Association for Computational Linguistics. URL <https://www.aclweb.org/anthology/2020.emnlp-demos.6>.
- Yilin Wu, Qian Zhang, and Zhiping Shen. Kalman filtering with multiplicative and additive noises. In *2016 12th World Congress on Intelligent Control and Automation (WCICA)*, pp. 483–487. IEEE, 2016.
- Da Yu, Saurabh Naik, Arturs Backurs, Sivakanth Gopi, Huseyin A Inan, Gautam Kamath, Janardhan Kulkarni, Yin Tat Lee, Andre Manoel, Lukas Wutschitz, et al. Differentially private fine-tuning of language models. In *International Conference on Learning Representations*, 2021.

Manzil Zaheer, Sashank Reddi, Devendra Sachan, Satyen Kale, and Sanjiv Kumar. Adaptive methods for nonconvex optimization. *Advances in neural information processing systems*, 31, 2018.

Jiaqi Zhang, Kai Zheng, Wenlong Mou, and Liwei Wang. Efficient private erm for smooth objectives. In *Proceedings of the 26th International Joint Conference on Artificial Intelligence*, pp. 3922–3928, 2017.

Xinwei Zhang, Mingyi Hong, and Nicola Elia. Understanding a class of decentralized and federated optimization algorithms: A multirate feedback control perspective. *SIAM Journal on Optimization*, 33(2):652–683, 2023.

Xinwei Zhang, Zhiqi Bu, Mingyi Hong, and Meisam Razaviyayn. Doppler: Differentially private optimizers with low-pass filter for privacy noise reduction. *arXiv preprint arXiv:2408.13460*, 2024a.

Xinwei Zhang, Zhiqi Bu, Steven Wu, and Mingyi Hong. Differentially private sgd without clipping bias: An error-feedback approach. In *The Twelfth International Conference on Learning Representations*, 2024b.

A ADDITIONAL DISCUSSION

A.1 BACKGROUND ON KALMAN FILTER

In this section, we provide an introduction and derivation of the Kalman filter. Kalman filter is introduced in (Kalman, 1960) and widely used for control systems in accurately estimating system states with noisy observation and known system dynamics. Kalman filter assumes the system is a linear (time-invariant) system:

$$\boldsymbol{\theta}_t = \mathbf{A}\boldsymbol{\theta}_{t-1} + \mathbf{u}_t + \mathbf{v}_t, \quad (\text{System update})$$

$$\boldsymbol{\psi}_t = \mathbf{C}\boldsymbol{\theta}_t + \mathbf{w}_t, \quad (\text{Observation})$$

where \mathbf{A}, \mathbf{C} are known matrix, and $\mathbf{v}_t \sim \mathcal{N}(0, \Sigma_{\mathbf{v}})$, $\mathbf{w}_t \sim \mathcal{N}(0, \Sigma_{\mathbf{w}})$ follows Gaussian distributions with known covariance matrices $\Sigma_{\mathbf{v}}, \Sigma_{\mathbf{w}}$, and \mathbf{u}_t is known input signal. The goal of the Kalman filter is to estimate $\boldsymbol{\theta}_t$ with the observation of $\boldsymbol{\psi}_t$ with the least mean-square error.

Derivation: First, we denote the estimation of $\boldsymbol{\theta}_t$ as $\tilde{\boldsymbol{\theta}}_t$, and the covariance of $\boldsymbol{\theta}_t - \tilde{\boldsymbol{\theta}}_t$ as

$$\mathbf{P}_t = \mathbb{E}[(\boldsymbol{\theta}_t - \tilde{\boldsymbol{\theta}}_t)(\boldsymbol{\theta}_t - \tilde{\boldsymbol{\theta}}_t)^\top],$$

Then, the system dynamics give an unbiased prediction:

$$\tilde{\boldsymbol{\theta}}_{t|t-1} = \mathbf{A}\tilde{\boldsymbol{\theta}}_{t-1} + \mathbf{u}_t, \quad (11)$$

and its covariance is

$$\mathbf{P}_{t|t-1} = \mathbb{E}[(\boldsymbol{\theta}_t - \tilde{\boldsymbol{\theta}}_{t|t-1})(\boldsymbol{\theta}_t - \tilde{\boldsymbol{\theta}}_{t|t-1})^\top] = \mathbf{A}\mathbf{P}_{t-1}\mathbf{A}^\top + \Sigma_{\mathbf{v}}. \quad (12)$$

With $\tilde{\boldsymbol{\theta}}_{t|t-1}$, we have the prediction error $\Delta\boldsymbol{\psi}_t = \boldsymbol{\psi}_t - \mathbf{C}\tilde{\boldsymbol{\psi}}_{t|t-1}$. Since the system is linear, we would like to use the prediction error to correct the prediction:

$$\tilde{\boldsymbol{\theta}}_t = \tilde{\boldsymbol{\theta}}_{t|t-1} + \mathbf{K}_t\Delta\boldsymbol{\psi}_t = \mathbf{K}_t\boldsymbol{\psi}_t + (\mathbf{I} - \mathbf{K}_t\mathbf{C})\tilde{\boldsymbol{\theta}}_{t|t-1}. \quad (13)$$

The goal of the Kalman filter is to minimize the mean-square error: $\min_{\mathbf{K}} \mathbb{E}[\|\boldsymbol{\theta}_t - \tilde{\boldsymbol{\theta}}_t\|^2]$, which is equivalent to minimizing $\text{tr}(\mathbf{P}_t)$. From the definition of $\tilde{\boldsymbol{\theta}}_t$, we have:

$$\begin{aligned} \mathbf{P}_t &= \mathbb{E}[(\boldsymbol{\theta}_t - \tilde{\boldsymbol{\theta}}_t)(\boldsymbol{\theta}_t - \tilde{\boldsymbol{\theta}}_t)^\top] \\ &= \mathbb{E}[(\boldsymbol{\theta}_t - \mathbf{K}_t\boldsymbol{\psi}_t + (\mathbf{I} - \mathbf{K}_t\mathbf{C})\tilde{\boldsymbol{\theta}}_{t|t-1})(\boldsymbol{\theta}_t - \mathbf{K}_t\boldsymbol{\psi}_t + (\mathbf{I} - \mathbf{K}_t\mathbf{C})\tilde{\boldsymbol{\theta}}_{t|t-1})^\top] \\ &= \mathbb{E}[(\boldsymbol{\theta}_t - \tilde{\boldsymbol{\theta}}_{t|t-1} - \mathbf{K}_t\mathbf{C}(\boldsymbol{\theta}_t - \tilde{\boldsymbol{\theta}}_{t|t-1}) - \mathbf{K}_t\mathbf{w}_t)(\boldsymbol{\theta}_t - \tilde{\boldsymbol{\theta}}_{t|t-1} - \mathbf{K}_t\mathbf{C}(\boldsymbol{\theta}_t - \tilde{\boldsymbol{\theta}}_{t|t-1}) - \mathbf{K}_t\mathbf{w}_t)^\top] \\ &= \mathbf{P}_{t|t-1} - \mathbf{K}_t\mathbf{C}\mathbf{P}_{t|t-1} - (\mathbf{K}_t\mathbf{C}\mathbf{P}_{t|t-1})^\top + \mathbf{K}_t(\mathbf{C}\mathbf{P}_{t|t-1}\mathbf{C}^\top + \Sigma_{\mathbf{w}})\mathbf{K}_t^\top. \end{aligned}$$

Taking partial derivative to the trace of \mathbf{P}_t with respect to \mathbf{K}_t , and set it to zero, we have:

$$\frac{\partial \text{tr}(\mathbf{P}_t)}{\partial \mathbf{K}_t} = -2(\mathbf{C}\mathbf{P}_{t|t-1})^\top + 2(\mathbf{C}\mathbf{P}_{t|t-1}\mathbf{C}^\top + \Sigma_{\mathbf{w}})\mathbf{K}_t^\top = 0,$$

which gives

$$\mathbf{K}_t = \mathbf{P}_{t|t-1}\mathbf{C}^\top(\mathbf{C}\mathbf{P}_{t|t-1}\mathbf{C}^\top + \Sigma_{\mathbf{w}})^{-1}. \quad (14)$$

Substitute \mathbf{K}_t back to \mathbf{P}_t , we can simplify

$$\begin{aligned} \mathbf{P}_t &= \mathbf{P}_{t|t-1} - \mathbf{K}_t\mathbf{C}\mathbf{P}_{t|t-1} - (\mathbf{K}_t\mathbf{C}\mathbf{P}_{t|t-1})^\top + \mathbf{K}_t(\mathbf{C}\mathbf{P}_{t|t-1}\mathbf{C}^\top + \Sigma_{\mathbf{w}})\mathbf{K}_t^\top \\ &= \mathbf{P}_{t|t-1} - \mathbf{K}_t\mathbf{C}\mathbf{P}_{t|t-1} = (\mathbf{I} - \mathbf{K}_t\mathbf{C})\mathbf{P}_{t|t-1}. \end{aligned} \quad (15)$$

Combining (11)-(15) together, we have the update of the Kalman filter:

$$\begin{aligned}\tilde{\boldsymbol{\theta}}_{t|t-1} &= \mathbf{A}\tilde{\boldsymbol{\theta}}_{t-1} + \mathbf{u}_t \\ \mathbf{P}_{t|t-1} &= \mathbf{A}\mathbf{P}_{t-1}\mathbf{A}^\top + \Sigma_{\mathbf{v}} \\ \mathbf{K}_t &= \mathbf{P}_{t|t-1}\mathbf{C}^\top (\mathbf{C}\mathbf{P}_{t|t-1}\mathbf{C}^\top + \Sigma_{\mathbf{w}})^{-1} \\ \tilde{\boldsymbol{\theta}}_t &= (\mathbf{I} - \mathbf{K}_t\mathbf{C})\tilde{\boldsymbol{\theta}}_{t|t-1} + \mathbf{K}_t\boldsymbol{\psi}_t \\ \mathbf{P}_t &= (\mathbf{I} - \mathbf{K}_t\mathbf{C})\mathbf{P}_{t|t-1}.\end{aligned}$$

Variants of Kalman filter: Kalman filter is designed for estimating the states following linear dynamics and achieves optimal performance, i.e., gives the smallest mean square error of the estimation when the system is linear (Welch et al., 1995). Extended Kalman filter (EKF) and unscented Kalman filter (UKF) are developed to deal with non-linear systems. EKF linearizes the non-linear system at each step and performs the Kalman filter on the linearized system (Ribeiro, 2004), while UKF takes the effect of the system non-linearity to the noise distribution into consideration and applies the unscented transform on the noise distribution and applies the Kalman filter on the system and the noise distribution (Wan & Van Der Merwe, 2001). Other extensions of the Kalman filter have been developed for special cases, including multiplicative noise and noisy input \mathbf{u}_t (Wu et al., 2016).

A.2 OTHER SYSTEM DYNAMICS FOR DPSGD

In this section, we want to discuss other possible formulations of the system dynamics for DPSGD to apply the Kalman filter.

Optimization variable and gradient version 1: Other than only using the gradients' dynamics in the main paper, we can construct the system taking the dynamics of the optimization variable \mathbf{x} into the system (Vuckovic, 2018):

$$\begin{bmatrix} \mathbf{x}_{t+1} \\ \nabla F(\mathbf{x}_{t+1}) \end{bmatrix} = \begin{bmatrix} \mathbf{I} & -\eta\mathbf{I} \\ 0 & \mathbf{I} \end{bmatrix} \begin{bmatrix} \mathbf{x}_t \\ \nabla F(\mathbf{x}_t) \end{bmatrix} + \begin{bmatrix} \eta\mathbf{w}_t \\ 0 \end{bmatrix},$$

$$\mathbf{y}_t = \mathbf{x}_t.$$

However, this dynamic is inaccurate as the dynamics of the gradient are simplified to $\nabla F(\mathbf{x}_{t+1}) = \nabla F(\mathbf{x}_t)$. Although the update can further incorporate with the momentum methods, i.e., by adding a momentum \mathbf{m}_t into the system, it fails to reveal the actual dynamic of the system.

Optimization variable and gradient version 2: Instead of treating the gradient as a constant, we can further utilize the Hessian to reveal the gradient dynamics:

$$\begin{bmatrix} \mathbf{x}_{t+1} \\ \mathbf{x}_t \\ \nabla F(\mathbf{x}_t) \end{bmatrix} = \begin{bmatrix} \mathbf{I} - \eta\mathbf{H} & \eta\mathbf{H} & -\eta\mathbf{I} \\ \mathbf{I} & 0 & 0 \\ \mathbf{H} & -\mathbf{H} & \mathbf{I} \end{bmatrix} \begin{bmatrix} \mathbf{x}_t \\ \mathbf{x}_{t-1} \\ \nabla F(\mathbf{x}_{t-1}) \end{bmatrix} + \begin{bmatrix} \eta\mathbf{w}_t \\ 0 \\ 0 \end{bmatrix},$$

$$\mathbf{y}_t = \mathbf{x}_t.$$

This system is more accurate in evaluating the gradient at the cost of using an extra \mathbf{x}_{t-1} state and a larger transition matrix. For non-linear problems $F(\mathbf{x})$, where \mathbf{H} is not a constant, we can apply the extended Kalman filter and replace \mathbf{H} with \mathbf{H}_t that linearizes the problem at each time step.

Gradient and Hessian: In work (Bittner & Pronzato, 2004), the dynamics of the gradient and Hessian have been used to construct the system:

$$\begin{bmatrix} \nabla F(\mathbf{x}_{t+1}) \\ \mathbf{h}_{t+1} \end{bmatrix} = \begin{bmatrix} \mathbf{I} & \Delta\mathbf{X}_t \\ 0 & \mathbf{I} \end{bmatrix} \begin{bmatrix} \nabla F(\mathbf{x}_t) \\ \mathbf{h}_t \end{bmatrix},$$

$$\mathbf{g}_t = \nabla F(\mathbf{x}_t) + \mathbf{w}_t,$$

where $\mathbf{h}_t = [\mathbf{H}_{1,1}, \dots, \mathbf{H}_{i,i+j}, \dots, \mathbf{H}_{d,d}]^\top$, with $j \in [0, \dots, d-i]$ represents the entries in the upper triangular part of the Hessian matrix. $\Delta\mathbf{X}_t$ is constructed such that $\Delta\mathbf{X}_t\mathbf{h}_t = \mathbf{H}_t(\mathbf{x}_{t+1} - \mathbf{x}_t)$. The system treats the Hessian matrix as a constant matrix, and the transition matrix is of size $(d + d(d-1)/2) \times d + d(d-1)/2$.

Although there are different ways to construct the Kalman filter for gradient noise reduction, the above systems are not implementable in practical deep-learning applications. Because the transition matrices of these systems are non-diagonal, the Kalman filters have non-diagonal gain \mathbf{K}_t and \mathbf{P}_t . Therefore, the matrix inversion operation is unavoidable when Kalman filters are implemented based

on these systems. The computation complexity for the matrix inversion can be $\mathcal{O}(d^3)$ to $\mathcal{O}(d^6)$, and the memory consumption is $\mathcal{O}(d^2)$ to $\mathcal{O}(d^4)$ for storing the matrices of the Kalman filter.

A.3 ALGORITHM SIMPLIFICATION

In this section, we explain how the simplification proceeds from Algorithm 2 to Algorithm 3. Recall that updates of Algorithm 2 is

$$\tilde{\mathbf{g}}_{t|t-1} = \tilde{\mathbf{g}}_{t-1} + \tilde{\mathbf{H}}_t(\mathbf{x}_t - \mathbf{x}_{t-1}) \quad (\text{Prediction})$$

$$\mathbf{P}_{t|t-1} = \mathbf{P}_{t-1} + \Sigma_{\mathbf{H}} + \Sigma_{\mathbf{v}}$$

$$\begin{aligned} \mathbf{K}_t &= \mathbf{P}_{t|t-1} \mathbb{E}[\mathbf{C}_t]^\top (\Sigma_{\mathbf{w}} + \mathbb{E}[\mathbf{C}_t] (\Sigma_{\mathbf{C}} \mathbf{S}_t + \mathbf{P}_{t|t-1}) \mathbb{E}[\mathbf{C}_t]^\top - \Sigma_{\mathbf{H}})^{-1} \\ \tilde{\mathbf{g}}_t &= \tilde{\mathbf{g}}_{t|t-1} + \mathbf{K}_t(\mathbf{g}_t - \mathbb{E}[\mathbf{C}_t] \tilde{\mathbf{g}}_{t|t-1}) \end{aligned} \quad (\text{Correction})$$

$$\mathbf{P}_t = (\mathbf{I} - \mathbf{K}_t \mathbb{E}[\mathbf{C}_t]) \mathbf{P}_{t|t-1}$$

$$\mathbf{S}_t = \mathbb{E}[\tilde{\mathbf{g}}_t \tilde{\mathbf{g}}_t^\top],$$

where $\mathbf{g}_t = \frac{1}{B} \sum_{\xi \in \mathcal{B}_t} \text{clip}(\nabla f(\mathbf{x}_t; \xi), C) + \mathbf{w}_t$. We apply four steps of simplification, including

1. Replacing random \mathbf{C}_t with constant \mathbf{I}_d .
2. Use finite difference to estimate $\mathbf{H}_t \mathbf{d}_{t-1}$.
3. Replace $\Sigma_{\mathbf{H}}$ with diagonal matrix $\sigma_H^2 \mathbf{I}_d$, $\Sigma_{\mathbf{v}}$ with $\sigma_v^2 \mathbf{I}_d$, and $\Sigma_{\mathbf{w}}$ with $\sigma_w^2 \mathbf{I}_d$.
4. Use fixed filter gain κ .

Step 1. By replacing \mathbf{C}_t with \mathbf{I}_d , and $\Sigma_{\mathbf{C}} = 0$, the update becomes

$$\tilde{\mathbf{g}}_{t|t-1} = \tilde{\mathbf{g}}_{t-1} + \tilde{\mathbf{H}}_t(\mathbf{x}_t - \mathbf{x}_{t-1}) \quad (\text{Prediction})$$

$$\mathbf{P}_{t|t-1} = \mathbf{P}_{t-1} + \Sigma_{\mathbf{H}} + \Sigma_{\mathbf{v}}$$

$$\mathbf{K}_t = \mathbf{P}_{t|t-1} (\Sigma_{\mathbf{w}} + \mathbf{P}_{t|t-1} - \Sigma_{\mathbf{H}})^{-1}$$

$$\tilde{\mathbf{g}}_t = \tilde{\mathbf{g}}_{t|t-1} + \mathbf{K}_t(\mathbf{g}_t - \tilde{\mathbf{g}}_{t|t-1}) \quad (\text{Correction})$$

$$\mathbf{P}_t = (\mathbf{I} - \mathbf{K}_t) \mathbf{P}_{t|t-1}.$$

Step 2. By using the finite difference to estimate $\mathbf{H}_t \mathbf{d}_{t-1}$, the prediction step becomes:

$$\tilde{\mathbf{g}}_{t|t-1} = \tilde{\mathbf{g}}_{t-1} + \frac{1}{B} \sum_{\xi \in \mathcal{B}_t} \frac{\nabla f(\mathbf{x}_t + \gamma \mathbf{d}_{t-1}; \xi) - \nabla f(\mathbf{x}_t; \xi)}{\gamma} \quad (\text{Prediction}).$$

Step 3. By replacing Σ 's with diagonal matrix $\sigma^2 \mathbf{I}_d$'s, the update becomes:

$$\tilde{\mathbf{g}}_{t|t-1} = \tilde{\mathbf{g}}_{t-1} + \frac{1}{B} \sum_{\xi \in \mathcal{B}_t} \frac{\nabla f(\mathbf{x}_t + \gamma \mathbf{d}_{t-1}; \xi) - \nabla f(\mathbf{x}_t; \xi)}{\gamma} \quad (\text{Prediction})$$

$$p_{t|t-1} = p_{t-1} + \sigma_H^2 + \sigma_v^2, \mathbf{P}_{t|t-1} = p_{t|t-1} \mathbf{I}_d$$

$$k_t = \frac{p_{t|t-1}}{p_{t|t-1} + \sigma_w^2 - \sigma_H^2} = \frac{p_{t-1} + \sigma_H^2 + \sigma_v^2}{p_{t-1} + \sigma_w^2 + \sigma_v^2}, \mathbf{K}_t = k_t \mathbf{I}_d$$

$$\tilde{\mathbf{g}}_t = \tilde{\mathbf{g}}_{t|t-1} + k_t(\mathbf{g}_t - \tilde{\mathbf{g}}_{t|t-1}) \quad (\text{Correction})$$

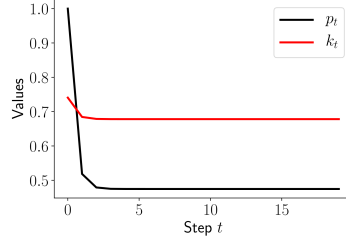
$$p_t = (1 - k_t) p_{t|t-1} = \frac{(\sigma_w^2 - \sigma_H^2)(p_{t-1} + \sigma_H^2 + \sigma_v^2)}{p_{t-1} + \sigma_w^2 + \sigma_v^2}.$$

Step 4. As discussed in the main paper, the update of k_t, p_t becomes:

$$k_t = \frac{p_{t-1} + \sigma_H^2 + \sigma_v^2}{p_{t-1} + \sigma_w^2 + \sigma_v^2},$$

$$p_t = \frac{(\sigma_w^2 - \sigma_H^2)(p_{t-1} + \sigma_H^2 + \sigma_v^2)}{p_{t-1} + \sigma_w^2 + \sigma_v^2}.$$

Therefore, p_t converges to $p_\infty = \frac{\sqrt{\sigma_H^2 + \sigma_v^2} \sqrt{4\sigma_w^2 - 3\sigma_H^2 + \sigma_v^2} - (\sigma_H^2 + \sigma_v^2)}{2}$, k_t converges to $k_\infty = \frac{p_\infty + \sigma_H^2 + \sigma_v^2}{p_\infty + \sigma_w^2 + \sigma_v^2}$, with rate $c_k = \frac{2\sigma_w^2 + 3\sigma_H^2 + \sigma_v^2 - \sqrt{(\sigma_v^2 + \sigma_H^2)(4\sigma_w^2 + \sigma_v^2 - 3\sigma_H^2)}}{2\sigma_w^2 + 3\sigma_H^2 + \sigma_v^2 + \sqrt{(\sigma_v^2 + \sigma_H^2)(4\sigma_w^2 + \sigma_v^2 - 3\sigma_H^2)}}$.

Figure 3: Convergence of k_t, p_t .

Therefore, we define $\kappa = k_\infty$ and replace k_t with κ , and the update becomes:

$$\tilde{\mathbf{g}}_{t|t-1} = \tilde{\mathbf{g}}_{t-1} + \frac{1}{B} \sum_{\xi \in \mathcal{B}_t} \frac{\nabla f(\mathbf{x}_t + \gamma \mathbf{d}_{t-1}; \xi) - \nabla f(\mathbf{x}_t; \xi)}{\gamma} \quad (\text{Prediction})$$

$$\tilde{\mathbf{g}}_t = \tilde{\mathbf{g}}_{t|t-1} + \kappa(\mathbf{g}_t - \tilde{\mathbf{g}}_{t|t-1}) \quad (\text{Correction})$$

Rearrange the terms, we have:

$$\begin{aligned} \tilde{\mathbf{g}}_t &= (1 - \kappa)\tilde{\mathbf{g}}_t + \kappa\mathbf{g}_t + (1 - \kappa)\frac{1}{B} \sum_{\xi \in \mathcal{B}_t} \frac{\nabla f(\mathbf{x}_t + \gamma \mathbf{d}_{t-1}; \xi) - \nabla f(\mathbf{x}_t; \xi)}{\gamma} \\ &= (1 - \kappa)\tilde{\mathbf{g}}_t + \kappa\hat{\mathbf{g}}_t, \text{ with} \\ \hat{\mathbf{g}}_t &= \mathbf{g}_t + \frac{1 - \kappa}{\kappa} \frac{1}{B} \sum_{\xi \in \mathcal{B}_t} \frac{\nabla f(\mathbf{x}_t + \gamma \mathbf{d}_{t-1}; \xi) - \nabla f(\mathbf{x}_t; \xi)}{\gamma} \\ &= \frac{1}{B} \sum_{\xi \in \mathcal{B}_t} \left(\frac{1 - \kappa}{\kappa\gamma} \nabla f(\mathbf{x}_t + \gamma \mathbf{d}_{t-1}; \xi) + \left(1 - \frac{1 - \kappa}{\kappa\gamma}\right) \nabla f(\mathbf{x}_t; \xi) \right) + \mathbf{w}_t, \end{aligned}$$

where we substitute $\mathbf{g}_t = \frac{1}{B} \sum_{\xi \in \mathcal{B}_t} \text{clip}(\nabla f(\mathbf{x}_t; \xi), C) + \mathbf{w}_t$. Then, by privatizing $\hat{\mathbf{g}}_t$ and rename it as \mathbf{g}_t , we have:

$$\mathbf{g}_t = \frac{1}{B} \sum_{\xi \in \mathcal{B}_t} \text{clip} \left(\frac{1 - \kappa}{\kappa\gamma} \nabla f(\mathbf{x}_t + \gamma \mathbf{d}_{t-1}; \xi) + \left(1 - \frac{1 - \kappa}{\kappa\gamma}\right) \nabla f(\mathbf{x}_t; \xi), C \right) + \mathbf{w}_t$$

$$\tilde{\mathbf{g}}_t = (1 - \kappa)\tilde{\mathbf{g}}_t + \kappa\mathbf{g}_t,$$

which is the update of Algorithm 3 (Lines 5 and 6).

A.4 CONNECTION BETWEEN DISK AND NAG AND STORM

Algorithm 3 has an implicit connection to the (unified) Nesterov Accelerated Gradient (NAG) method (Shen et al., 2023; Sutskever et al., 2013) and the Stochastic Recursive Momentum (STORM) algorithm (Cutkosky & Orabona, 2019). The update of (half-shifted) NAG can be written as (Sutskever et al., 2013):

$$\mathbf{m}_t = \mu\mathbf{m}_{t-1} + \eta\nabla F(\mathbf{x}_t - \mu\mathbf{m}_{t-1}) \quad (16)$$

$$\mathbf{x}_{t+1} = \mathbf{x}_t - \mathbf{m}_t,$$

and the update of STORM writes (Cutkosky & Orabona, 2019):

$$\mathbf{m}_t = (1 - \alpha)\mathbf{m}_{t-1} + \alpha\nabla f(\mathbf{x}_t, \xi_t) + (1 - \alpha)(\nabla f(\mathbf{x}_t, \xi_t) - \nabla f(\mathbf{x}_{t-1}, \xi_t)) \quad (17)$$

$$\mathbf{x}_{t+1} = \mathbf{x}_t - \eta\mathbf{m}_t,$$

In comparison, in Algorithm 3, by letting the update of OptimizerUpdate be SGD, and assuming clipping is inactive, $\mathbf{w}_t = 0$, i.e., without DP, $\epsilon \rightarrow \infty$, the DiSK becomes:

$$\begin{aligned} \tilde{\mathbf{g}}_t &= (1 - \kappa)\tilde{\mathbf{g}}_{t-1} + \frac{\kappa}{B} \sum_{\xi \in \mathcal{B}_t} \left(\frac{1 - \kappa}{\kappa\gamma} \nabla f(\mathbf{x}_t + \gamma \mathbf{d}_{t-1}; \xi) + \left(1 - \frac{1 - \kappa}{\kappa\gamma}\right) \nabla f(\mathbf{x}_t; \xi) \right) \\ &= (1 - \kappa)\tilde{\mathbf{g}}_{t-1} + \frac{\kappa}{B} \sum_{\xi \in \mathcal{B}_t} \nabla f(\mathbf{x}_t; \xi) + \frac{1 - \kappa}{B\gamma} \sum_{\xi \in \mathcal{B}_t} (\nabla f(\mathbf{x}_t + \gamma \mathbf{d}_{t-1}; \xi) - \nabla f(\mathbf{x}_t; \xi)) \quad (18) \end{aligned}$$

$$\mathbf{x}_{t+1} = \mathbf{x}_t - \eta\tilde{\mathbf{g}}_t.$$

Comparing the above updates, we observe that (16) and (17) are two special cases of (18) with specific choices of the parameters. Specifically, by letting $\gamma = \frac{1 - \kappa}{\kappa} > 0, \eta = \kappa, 1 - \kappa = \mu, B = N$, we have $1 - \frac{1 - \kappa}{\kappa\gamma} = 0$, and the update of $\tilde{\mathbf{g}}_t$ becomes $\tilde{\mathbf{g}}_t = \mu\tilde{\mathbf{g}}_{t-1} + \eta\nabla F(\mathbf{x}_t - \frac{\mu}{\eta}\tilde{\mathbf{g}}_{t-1})$, and DiSK

becomes NAG; on the other hand, by letting $\gamma = -1, \kappa = \alpha, B = 1$, we have $\mathbf{x}_t + \gamma \mathbf{d}_{t-1} = \mathbf{x}_t - (\mathbf{x}_t - \mathbf{x}_{t-1}) = \mathbf{x}_{t-1}$, and the update of $\tilde{\mathbf{g}}_t$ becomes $\tilde{\mathbf{g}}_t = (1 - \alpha)\tilde{\mathbf{g}}_{t-1} + \alpha \nabla f(\mathbf{x}_t; \xi_t) + (1 - \alpha)(\nabla f(\mathbf{x}_t; \xi) - \nabla f(\mathbf{x}_{t-1}; \xi))$, which matches the update of STORM. From this discussion, we see that NAG and STORM, two algorithms for accelerated gradient and variance reduction, respectively, can be unified by DiSK, an algorithm based on Kalman filtering.

With this discussion, we observe that the key difference between NAG and STORM is the choice of γ . When $\gamma > 0$, the algorithm is close to NAG, which focuses on “exploring” and “accelerating”. When $\gamma < 0$, the algorithm is close to STORM, which focuses on “exploiting” and “reducing noise”.

B PROOF FOR SECTION 4

In this section, we provide detailed proof for the results in Section 4.

We find the following relations useful:

$$\langle \mathbf{a}, \mathbf{b} \rangle \leq \frac{1}{2\alpha} \|\mathbf{a}\|^2 + \frac{\alpha}{2} \|\mathbf{b}\|^2, \quad (19)$$

$$\|\mathbf{a} + \mathbf{b}\|^2 \leq (1 + \alpha) \|\mathbf{a}\|^2 + (1 + 1/\alpha) \|\mathbf{b}\|^2. \quad (20)$$

In the following sections, we use \mathbb{E}_t to denote the expectation conditioned on all the information before iteration t . To prove Theorem 2, we first provide the following lemma to bound the difference between $\tilde{\mathbf{g}}_t$ and $\nabla F(\mathbf{x}_t)$. Let us define $\Delta_t = \nabla F(\mathbf{x}_t) - \tilde{\mathbf{g}}_t$. We have:

Lemma 1 Assume A1, A2 holds, we have:

$$\begin{aligned} \mathbb{E}_t \|\Delta_t\|^2 &\leq (1 - \kappa)^2 (1 + 4\eta^2 L^2 + |1 + \gamma| (\kappa + 2\eta^2 L^2 C_\gamma)) \|\Delta_{t-1}\|^2 \\ &\quad + 2\eta^2 L^2 (1 - \kappa)^2 (2 + |1 + \gamma| C_\gamma) \|\nabla F(\mathbf{x}_{t-1})\|^2 \\ &\quad + \kappa^2 \left((2 + |1 + \gamma|) \frac{\sigma_{SGD}^2}{B} + d\sigma_{DP}^2 \right), \end{aligned} \quad (21)$$

where we define $C_\gamma = \left(1 + \frac{4(2+1/\kappa+|1+\gamma|)}{\gamma^2}\right)$.

B.1 PROOF OF LEMMA 1

By the update of $\tilde{\mathbf{g}}_t$, we have:

$$\begin{aligned} &\mathbb{E}_t \|\Delta_t\|^2 \\ &= \mathbb{E}_t \left\| \nabla F(\mathbf{x}_t) - (1 - \kappa)\tilde{\mathbf{g}}_{t-1} - \frac{\kappa}{B} \sum_{\xi \in \mathcal{B}_t} \nabla f(\mathbf{x}_t, \xi) - \kappa \mathbf{w}_t \right. \\ &\quad \left. - \frac{1 - \kappa}{\gamma B} \sum_{\xi \in \mathcal{B}_t} (\nabla f(\mathbf{x}_t + \gamma \mathbf{d}_{t-1}; \xi) - \nabla f(\mathbf{x}_t; \xi)) \right\|^2 \\ &\stackrel{(a)}{=} \mathbb{E}_t \left\| (1 - \kappa)(\nabla F(\mathbf{x}_t) - \nabla F(\mathbf{x}_{t-1})) + (1 - \kappa)(\nabla F(\mathbf{x}_{t-1}) - \tilde{\mathbf{g}}_{t-1}) \right. \\ &\quad \left. + \kappa \left(\nabla F(\mathbf{x}_t) - \frac{1}{B} \sum_{\xi \in \mathcal{B}_t} \nabla f(\mathbf{x}_t, \xi) - \mathbf{w}_t \right) \right. \\ &\quad \left. - \frac{1 - \kappa}{\gamma B} \sum_{\xi \in \mathcal{B}_t} (\nabla f(\mathbf{x}_t + \gamma \mathbf{d}_{t-1}; \xi) - \nabla f(\mathbf{x}_t; \xi)) \right\|^2 \\ &\stackrel{(b)}{=} \mathbb{E}_t \left\| (1 - \kappa) \underbrace{\left(\nabla F(\mathbf{x}_t) - \nabla F(\mathbf{x}_{t-1}) - \frac{1}{B} \sum_{\xi \in \mathcal{B}_t} (\nabla f(\mathbf{x}_t; \xi) - \nabla f(\mathbf{x}_{t-1}; \xi)) \right)}_{:=D_1} \right\|^2 \end{aligned}$$

$$\begin{aligned}
& + (1 - \kappa)\Delta_{t-1} + \underbrace{\kappa \left(\nabla F(\mathbf{x}_t) - \frac{1}{B} \sum_{\xi \in \mathcal{B}_t} \nabla f(\mathbf{x}_t, \xi) \right)}_{:=D_2} - \kappa \mathbf{w}_t \\
& - (1 - \kappa) \underbrace{\frac{1}{B} \sum_{\xi \in \mathcal{B}_t} \left(\frac{1}{\gamma} \nabla f(\mathbf{x}_t + \gamma \mathbf{d}_{t-1}; \xi) + \nabla f(\mathbf{x}_{t-1} \mathbf{d}_{t-1}; \xi) - \frac{1+\gamma}{\gamma} \nabla f(\mathbf{x}_t; \xi) \right)}_{:=D_3} \Bigg\|^2 \\
& \stackrel{(c)}{=} (1 - \kappa)^2 \mathbb{E}_t \|D_1\|^2 + (1 - \kappa)^2 \|\Delta_{t-1}\|^2 + \kappa^2 \mathbb{E}_t [\|D_2\|^2] + (1 - \kappa)^2 \mathbb{E}_t \|D_3\|^2 + \kappa^2 \mathbb{E} [\|\mathbf{w}_t\|^2] \\
& \quad + 2(1 - \kappa)^2 \langle \mathbb{E}_t[D_1], \Delta_{t-1} \rangle + 2(1 - \kappa)\kappa \langle \mathbb{E}_t[D_2], \Delta_{t-1} \rangle - 2(1 - \kappa)^2 \langle \mathbb{E}_t[D_3], \Delta_{t-1} \rangle \\
& \quad + 2\mathbb{E}_t[\langle (1 - \kappa)D_1, \kappa D_2 \rangle] - 2(1 - \kappa)^2 \mathbb{E}_t[\langle D_1, D_3 \rangle] - 2\mathbb{E}_t[\langle \kappa D_2, (1 - \kappa)D_3 \rangle], \\
& \stackrel{(d)}{=} (1 - \kappa)^2 (2 + |1 + \gamma|) \mathbb{E}_t \|D_1\|^2 + (1 - \kappa)^2 (1 + \kappa |1 + \gamma|) \|\Delta_{t-1}\|^2 + \kappa^2 (2 + |1 + \gamma|) \mathbb{E}_t [\|D_2\|^2] \\
& \quad + (1 - \kappa)^2 \left(1 + \frac{2}{|1 + \gamma|} + \frac{1}{\kappa |1 + \gamma|} \right) \mathbb{E}_t \|D_3\|^2 + \kappa^2 d\sigma_{\text{DP}}^2, \tag{22}
\end{aligned}$$

where (a) we add and subtract $(1 - \kappa)\nabla F(\mathbf{x}_{t-1})$ and rearrange the terms; (b) adds and subtracts $\frac{1-\kappa}{B} \sum_{\xi \in \mathcal{B}_t} (\nabla f(\mathbf{x}_t; \xi) - \nabla f(\mathbf{x}_{t-1}; \xi))$; (c) directly expands the square; and in (d), we notice that $\mathbb{E}_t[D_1] = 0$, $\mathbb{E}_t[D_2] = 0$, so the first two inner products are zero, and we apply (19) to the other four inner products, with $\alpha = \kappa |1 + \gamma|$, 1 , $|1 + \gamma|$, respectively. Next, we bound each term separately. For $\mathbb{E}_t[\|D_1\|^2]$, we have:

$$\begin{aligned}
\mathbb{E}_t[\|D_1\|^2] &= \mathbb{E}_t \left\| \nabla F(\mathbf{x}_t) - \nabla F(\mathbf{x}_{t-1}) - \frac{1}{B} \sum_{\xi \in \mathcal{B}_t} (\nabla f(\mathbf{x}_t; \xi) - \nabla f(\mathbf{x}_{t-1}; \xi)) \right\|^2 \\
&\stackrel{(a)}{\leq} \mathbb{E}_t \left\| \frac{1}{B} \sum_{\xi \in \mathcal{B}_t} (\nabla f(\mathbf{x}_t; \xi) - \nabla f(\mathbf{x}_{t-1}; \xi)) \right\|^2 \\
&\stackrel{(b)}{\leq} L^2 \eta^2 \|\tilde{\mathbf{g}}_{t-1}\|^2 \\
&\stackrel{(c)}{\leq} 2L^2 \eta^2 (\|\Delta_{t-1}\|^2 + \|\nabla F(\mathbf{x}_{t-1})\|^2),
\end{aligned} \tag{23}$$

where (a) uses the fact that $\mathbb{E} \|X - \mathbb{E}[X]\|^2 \leq \mathbb{E} \|X\|^2$; (b) applies A1 and (c) adds and subtracts $\nabla F(\mathbf{x}_{t-1})$, and applies (20). For $\mathbb{E}_t[\|D_2\|^2]$, we have:

$$\mathbb{E}_t[\|D_2\|^2] = \mathbb{E}_t \left\| \nabla F(\mathbf{x}_t) - \frac{1}{B} \sum_{\xi \in \mathcal{B}_t} \nabla f(\mathbf{x}_t, \xi) \right\|^2 \stackrel{A2}{\leq} \frac{\sigma_{\text{SGD}}^2}{B}. \tag{24}$$

For $\mathbb{E}_t[\|D_3\|^2]$, we have:

$$\begin{aligned}
\mathbb{E}_t[\|D_3\|^2] &= \mathbb{E}_t \left\| \frac{1}{B} \sum_{\xi \in \mathcal{B}_t} \left(\frac{1}{\gamma} \nabla f(\mathbf{x}_t + \gamma \mathbf{d}_{t-1}; \xi) + \nabla f(\mathbf{x}_{t-1} \mathbf{d}_{t-1}; \xi) - \frac{1+\gamma}{\gamma} \nabla f(\mathbf{x}_t; \xi) \right) \right\|^2 \\
&\stackrel{(a)}{\leq} \frac{1}{B} \sum_{\xi \in \mathcal{B}_t} \left\| \frac{1}{\gamma} \nabla f(\mathbf{x}_t + \gamma \mathbf{d}_{t-1}; \xi) - \frac{1}{\gamma} \nabla f(\mathbf{x}_{t-1}; \xi) \right. \\
&\quad \left. + \frac{1+\gamma}{\gamma} \nabla f(\mathbf{x}_{t-1} \mathbf{d}_{t-1}; \xi) - \frac{1+\gamma}{\gamma} \nabla f(\mathbf{x}_t; \xi) \right\|^2 \\
&\stackrel{(20)}{\leq} 2 \left\| \frac{1}{\gamma} \nabla f(\mathbf{x}_t + \gamma \mathbf{d}_{t-1}; \xi) - \frac{1}{\gamma} \nabla f(\mathbf{x}_{t-1}; \xi) \right\|^2 \\
&\quad + 2 \left\| \frac{1+\gamma}{\gamma} \nabla f(\mathbf{x}_{t-1}; \xi) - \frac{1+\gamma}{\gamma} \nabla f(\mathbf{x}_t; \xi) \right\|^2
\end{aligned}$$

$$\begin{aligned}
&\stackrel{A1}{\leq} \frac{2L^2}{\gamma^2} \|\mathbf{x}_t + \gamma \mathbf{d}_{t-1} - \mathbf{x}_{t-1}\|^2 + \frac{2L^2(1+\gamma)^2}{\gamma^2} \|\mathbf{x}_{t-1} - \mathbf{x}_t\|^2 \\
&\stackrel{(b)}{=} \frac{4L^2(1+\gamma)^2\eta^2}{\gamma^2} \|\tilde{\mathbf{g}}_{t-1}\|^2 \\
&\stackrel{(c)}{\leq} \frac{8L^2(1+\gamma)^2\eta^2}{\gamma^2} (\|\Delta_{t-1}\|^2 + \|\nabla F(\mathbf{x}_{t-1})\|^2), \tag{25}
\end{aligned}$$

where (a) applies Jensens' inequality to $\|\cdot\|^2$, and we add and subtract $\frac{1}{\gamma} \nabla f(\mathbf{x}_{t-1}; \xi)$; (b) applies (20); (c) uses the fact that $\mathbf{d}_{t-1} = \mathbf{x}_t - \mathbf{x}_{t-1} = -\eta \tilde{\mathbf{g}}_{t-1}$; and (c) adds and subtracts $\nabla F(\mathbf{x}_{t-1})$, and applies (20). Plug in (23) – (25) to (22), we have:

$$\begin{aligned}
\mathbb{E}_t \|\Delta_t\|^2 &\leq (1-\kappa)^2 (2 + |1+\gamma|) \mathbb{E}_t \|D_1\|^2 + (1-\kappa)^2 (1+\kappa|1+\gamma|) \|\Delta_{t-1}\|^2 + \kappa^2 d\sigma_{\text{DP}}^2 \\
&\quad + \kappa^2 (2 + |1+\gamma|) \mathbb{E}_t [\|D_2\|^2] + (1-\kappa)^2 \left(1 + \frac{2}{|1+\gamma|} + \frac{1}{\kappa|1+\gamma|} \right) \mathbb{E}_t \|D_3\|^2 \\
&\leq (1-\kappa)^2 (1 + 4\eta^2 L^2 + |1+\gamma| (\kappa + 2\eta^2 L^2 C_\gamma)) \|\Delta_{t-1}\|^2 \\
&\quad + 2\eta^2 L^2 (1-\kappa)^2 (2 + |1+\gamma| C_\gamma) \|\nabla F(\mathbf{x}_{t-1})\|^2 \\
&\quad + \kappa^2 \left((2 + |1+\gamma|) \frac{\sigma_{\text{SGD}}^2}{B} + d\sigma_{\text{DP}}^2 \right), \tag{26}
\end{aligned}$$

where we define $C_\gamma := \left(1 + \frac{4(2+1/\kappa+|1+\gamma|)}{\gamma^2} \right)$. This completes the proof of Lemma 1.

B.2 PROOF OF THEOREM 2

Then, we are ready to prove Theorem 2. By choosing $C \geq G(1 + \frac{2(1-\kappa)}{\kappa\gamma})$, the clipping is inactive. Recall that from the update rule, we have

$$\begin{aligned}
\mathbb{E}_t[\tilde{\mathbf{g}}_t] &= (1-\kappa)\tilde{\mathbf{g}}_{t-1} + \kappa \nabla F(\mathbf{x}_t) + (1-\kappa)(\nabla F(\mathbf{x}_t) - \nabla F(\mathbf{x}_{t-1})) \\
&= \nabla F(\mathbf{x}_t) - (1-\kappa)\Delta_{t-1}. \tag{27}
\end{aligned}$$

Then, by A1, we have:

$$\begin{aligned}
\mathbb{E}_t[F(\mathbf{x}_{t+1})] - F(\mathbf{x}_t) &\leq -\eta \langle \nabla F(\mathbf{x}_t), \mathbb{E}_t[\tilde{\mathbf{g}}_t] \rangle + \frac{\eta^2 L}{2} \mathbb{E}_t \|\tilde{\mathbf{g}}_t\|^2 \\
&\stackrel{(a)}{=} -\eta \|\nabla F(\mathbf{x}_t)\|^2 + \eta(1-\kappa) \langle \nabla F(\mathbf{x}_t), \Delta_{t-1} \rangle + \frac{\eta^2 L}{2} \mathbb{E}_t \|\tilde{\mathbf{g}}_t\|^2 \\
&\stackrel{(b)}{\leq} -\frac{\eta(1+\kappa-2\eta L)}{2} \|\nabla F(\mathbf{x}_t)\|^2 + \frac{\eta(1-\kappa)}{2} \|\Delta_{t-1}\|^2 + \eta^2 L \mathbb{E}_t \|\Delta_t\|^2, \tag{28}
\end{aligned}$$

where (a) substitute (27); (b) applies (19) to the second term and we add and subtract $\nabla F(\mathbf{x}_t)$ to the last term and apply (20).

Define $\mathcal{L}_t := F(\mathbf{x}_t) + \beta \|\Delta_{t-1}\|^2$, we have:

$$\begin{aligned}
&\mathbb{E}_t[\mathcal{L}_{t+1}] - \mathcal{L}_t \\
&\leq -\frac{\eta(1+\kappa-2\eta L)}{2} \|\nabla F(\mathbf{x}_t)\|^2 - \left(\beta - \frac{\eta(1-\kappa)}{2} \right) \|\Delta_{t-1}\|^2 + (\beta + \eta^2 L) \mathbb{E}_t \|\Delta_t\|^2 \\
&\stackrel{(a)}{\leq} -\frac{\eta(1+\kappa-2\eta L)}{2} \|\nabla F(\mathbf{x}_t)\|^2 - \left(\beta - \frac{\eta(1-\kappa)}{2} \right) \|\Delta_{t-1}\|^2 \\
&\quad + (\beta + \eta^2 L)(1-\kappa)^2 (1 + 4L^2\eta^2 + |1+\gamma| (\kappa + 2\eta^2 L^2 C_\gamma)) \|\Delta_{t-1}\|^2 \\
&\quad + (\beta + \eta^2 L)\kappa^2 \left(\frac{(2 + |1+\gamma|)\sigma_{\text{SGD}}^2}{B} + d\sigma_{\text{DP}}^2 \right) \\
&\quad + 2(\beta + \eta^2 L)(1-\kappa)^2 L^2 \eta^2 (2 + |1+\gamma| C_\gamma) \|\nabla F(\mathbf{x}_{t-1})\|^2 \\
&= -\frac{\eta(1+\kappa-2\eta L)}{2} \|\nabla F(\mathbf{x}_t)\|^2 + 2(\beta + \eta^2 L)(1-\kappa)^2 L^2 \eta^2 (2 + |1+\gamma| C_\gamma) \|\nabla F(\mathbf{x}_{t-1})\|^2 \\
&\quad - \left(\beta - \frac{\eta(1-\kappa)}{2} - (\beta + \eta^2 L)(1-\kappa)^2 (1 + 4L^2\eta^2 + |1+\gamma| (\kappa + 2\eta^2 L^2 C_\gamma)) \right) \|\Delta_{t-1}\|^2 \\
&\quad + (\beta + \eta^2 L)\kappa^2 \left(\frac{(2 + |1+\gamma|)\sigma_{\text{SGD}}^2}{B} + d\sigma_{\text{DP}}^2 \right), \tag{29}
\end{aligned}$$

where (a) applies Lemma 1 and (b) rearrange the terms. By choosing

$$\eta < \frac{1}{2L(1 + 2(1 - \kappa)^2\beta L(2 + |1 + \gamma| C_\gamma))}, \quad \kappa > 1 - \frac{1}{\sqrt{1 + 4\eta^2 L^2 + |1 + \gamma| (\kappa + 2\eta^2 L^2 C_\gamma)}},$$

$$\beta \geq \frac{\eta(1 - \kappa)/2 + \eta^2 L(1 - \kappa)^2(1 + 4\eta^2 L^2 + |1 + \gamma| (\kappa + 2\eta^2 L^2 C_\gamma))}{1 - (1 - \kappa)^2(1 + 4\eta^2 L^2 + |1 + \gamma| (\kappa + 2\eta^2 L^2 C_\gamma))},$$

we have:

$$\frac{\eta(1 + \kappa - 2\eta L)}{2} - 2(\beta + \eta^2 L)(1 - \kappa)^2 L^2 \eta^2 (2 + |1 + \gamma| C_\gamma) > 0,$$

$$1 - (1 - \kappa)^2(1 + 4\eta^2 L^2 + |1 + \gamma| (\kappa + 2\eta^2 L^2 C_\gamma)) > 0, \quad (30)$$

$$\beta - \frac{\eta(1 - \kappa)}{2} - (\beta + \eta^2 L)(1 - \kappa)^2(1 + 4\eta^2 L^2 + |1 + \gamma| (\kappa + 2\eta^2 L^2 C_\gamma)) \geq 0.$$

Average from $t = 0$ to $T - 1$ and rearrange the terms, we have:

$$\frac{1}{T} \sum_{t=0}^T \mathbb{E} \|\nabla F(\mathbf{x}_t)\|^2 \leq \frac{2(\mathcal{L}_0 - \mathbb{E}[\mathcal{L}_{T+1}])}{C_1 \eta T} + \frac{2(\beta + \eta^2 L) \kappa^2}{C_1 \eta} \left(\frac{(2 + |1 + \gamma|) \sigma_{\text{SGD}}^2}{B} + d\sigma_{\text{DP}}^2 \right)$$

$$\leq \frac{2(F(\mathbf{x}_0) + \beta \|\nabla F(\mathbf{x}_0)\|^2 - F^*)}{C_1 \eta T} + \frac{2(\beta + \eta^2 L) \kappa^2}{C_1 \eta} \left(\frac{(2 + |1 + \gamma|) \sigma_{\text{SGD}}^2}{B} + d\sigma_{\text{DP}}^2 \right), \quad (31)$$

where we define $C_1 := (1 + \kappa - 2\eta L) - 4(\beta + \eta^2 L)(1 - \kappa)^2 L^2 \eta (2 + |1 + \gamma| C_\gamma)$, and in the last inequality we notice that $\mathcal{L}_{T+1} = F(\mathbf{x}_{T+1}) + \beta \|\Delta_T\|^2 \geq F^*$, and $\mathcal{L}_0 = F(\mathbf{x}_0) + \beta \|\nabla F(\mathbf{x}_0)\|^2$, as we initialize $\tilde{\mathbf{g}}_0 = 0$. This completes the proof of Theorem 2.

On the choice of $\gamma = -1$. From the above proof, we see that in Appendix B.1, (22) (c), we directly apply (19) to upper bound the cross-product terms by positive terms for the worst case, which results in the optimal choice of $\gamma = -1$. However, the inner products may be smaller than zero in some cases, making $\gamma = -1$ sub-optimal in practice.

C ADDITIONAL NUMERICAL RESULTS

C.1 EXPERIMENT DETAILS

Coding: The code for the experiments will be provided online. We use PyTorch as the code base and the FastDP package (Bu et al., 2023) to privatize the optimizers. The Algorithm 3 is implemented as a PyTorch optimizer, which can be easily combined with any training scripts based on PyTorch. The modification is minimum:

```

1 from KFOptimizer import KFOptimizer
2 # define base optimizer
3 optimizer = KFOptimizer(model.parameters(), base_optimizer, kappa, gamma)
4 # ...
5 # in training loop:
6     def closure(): # warp up the loss and backward computation
7         loss = model(input)
8         loss.backward()
9         return loss
10    loss = optimizer.prestep(closure)
11    # ...

```

The link to the full code of the experiments can be found at <https://anonymous.4open.science/r/KalmanDP-BEDB>.

Hardware: All the experiments except the ImageNet-1k dataset are running with one Nvidia A40 (48GB memory) or one Nvidia V100 (32GB memory). The experiment on the ImageNet-1k dataset is running on one Nvidia H100 (80GB memory) GPU. The training time varies for different tasks depending on the data size and model size.

Training method: We use gradient accumulation to deal with the large batch size and use learning rate warm-up for 1/20 of the training steps when training from randomly initialized weights. We

also use the Cosine Annealing learning rate scheduler (Loshchilov & Hutter, 2022), which gradually decreases the learning rate.

C.2 CHOICE OF HYPER-PARAMETERS

The main hyper-parameters in the algorithms are: epoch E , batch size B , step size η , clipping threshold C , Kalman filter parameters κ , and γ . In all experiments, we fix the clipping method as automatic clipping used in Bu et al. (2024), i.e., $\text{clip}(\nabla f(\mathbf{x}; \xi), C) = \nabla f(\mathbf{x}; \xi) \cdot \frac{C}{\|\nabla f(\mathbf{x}; \xi)\|}$, and set $C = 1$ for all experiments.

For each set of experiments, we conduct a grid search on the hyper-parameters E, B, η and choose the optimal ones for the DP optimizer without DiSK. The search grids of each hyper-parameter are listed in Table 2;

Table 2: Search grid of the CV pre-training experiments, the optimal hyper-parameters are in **bold**.

	Search grid		
	MNIST	CIFAR	ImageNet
E	$\{1, \mathbf{2}, 3\} \times 20$	$\{1, \mathbf{2}, 3, 4\} \times 40$	$\{3, \mathbf{4}\} \times 40$
B	$\{2, \mathbf{5}\} \times 10^3$	$\{0.5, 1, 2, \mathbf{5}\} \times 10^3$	$\{\mathbf{5}, 10\} \times 10^3$
η	$\{3, \mathbf{2.5}, 1, 0.3, 0.1\} \times 10^{-1}$	$\{1, 3, \mathbf{5}, 7, 10\} \times 10^{-3}$	$\{10, 3, 1, \mathbf{0.3}, 0.1\} \times 10^{-3}$
κ	$\{\mathbf{0.7}\}$	$\{9.9, 9, 8, \mathbf{7}, 6, 5\} \times 10^{-1}$	$\{\mathbf{0.7}\}$
γ	$\{\mathbf{0.5}\}$	$\{0.2, 0.3, \mathbf{0.5}, 1, 2, 3, \frac{1-\kappa}{\kappa}\}$	$\{\mathbf{0.5}\}$

Then, we fix E, B, η and conduct the ablation study on κ, γ as shown in Figure 8.

C.3 ADDITIONAL EXPERIMENTS ON CV TASKS

Training different models from scratch: We additionally train the WRN-16-4 and the ViT-small models on the CIFAR-10 with randomly initialized weights for different privacy budgets, and the test accuracies during the training are shown in Figure 4 for $\epsilon = 4$. From the results, we can see that DiSK consistently outperforms the base optimizer.

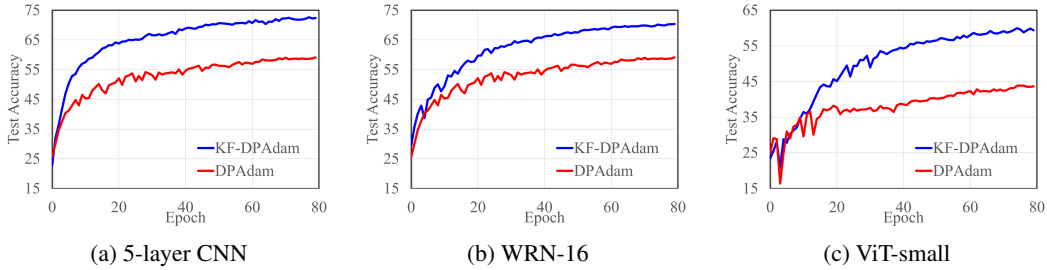


Figure 4: Test accuracy of pre-training 5-layer CNN, WRN-16, and ViT-small on CIFAR-10 dataset with and without DiSK for fixed privacy budget $\epsilon = 4$.

Fine-tuning on CIFAR-100: Besides training from scratch, we also compare the performance of fine-tuning a pre-trained ViT-small model on the CIFAR-100 dataset. The results for different ϵ are shown in Figure 5. For fine-tuning on the complex CIFAR-100 dataset, DiSK still improves the performance compared with DPAdam, and has less performance drop under large DP noise.

Comparison with existing methods and SOTA: We conduct comparisons with existing approaches for improving DP training performance. In Figure 6a, we train a linear regression model with synthetic data and compared the performance of Noisy GD, Noisy GD with DOPPLER (NoisyLP), and with DiSK (NoisyKF). We inject Gaussian noise with different variances into the gradient and compare the final performance. We observe that DiSK has the lowest regression loss under all noise levels, indicating that the Kalman filter performs better in noise reduction than the Low-pass filter. In Figure 6b, we compare the test accuracy of different methods, including DOPPLER (Zhang et al., 2024a) and DP-FTRL (Kairouz et al., 2021; Choquette-Choo et al., 2024) on the CIFAR-10

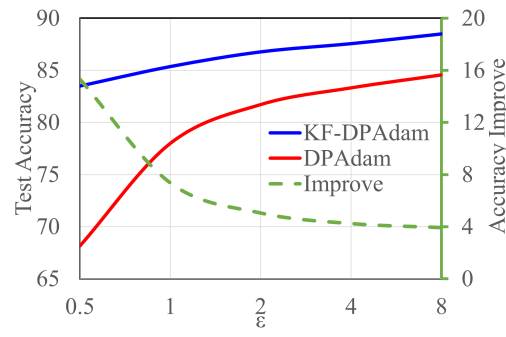
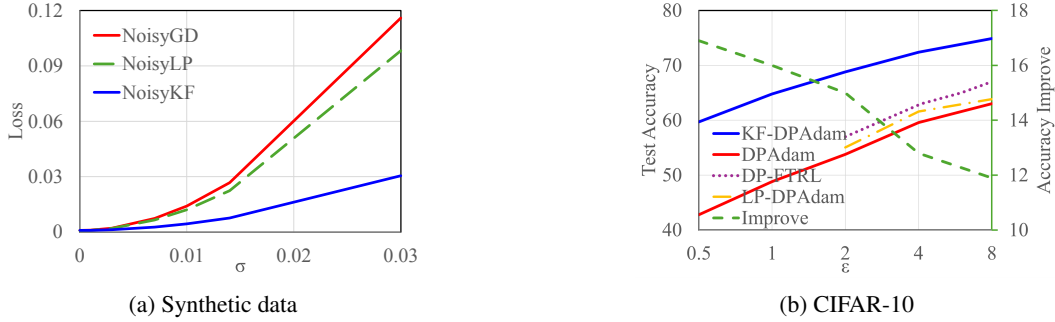
Figure 5: Fine-tuning ViT-small on CIFAR-100 with different ϵ .

Figure 6: Comparison with existing approaches. a) Kalman filter and low-pass filter; b) Kalman filter, DP-FTRL, and low-pass filter.

dataset training the WRN from scratch. We observe that DiSK significantly outperforms the SOTA algorithms on all privacy budgets.

Comparison with SOTA on ImageNet: Additionally, we conduct experiments to compare the performance of DiSK with SOTA result training from scratch on the ImageNet-1k dataset in De et al. (2022). The result is shown in Figure 7. We note that the reported test accuracy in the De et al. (2022) is 32.4% for privacy level $\epsilon = 8$. However, we noticed that their accounting procedure has been improved in their GitHub repository and hence we re-ran their experiment using the new accountant to obtain our baseline. We kept all their options on, including group normalization, larger batch size, weight standardization, augmentation multiplicity, and model exponential moving average. In addition, we also follow their *normalized clipping* strategy, i.e.,

$$\text{clip}(\nabla f, C) = \frac{\nabla f}{C} \min \left\{ \frac{C}{\|\nabla f\|}, 1 \right\}.$$

Their updated code results in 36.35% validation accuracy and the test accuracy of 33.56% (as the SOTA result). In comparison, adding DiSK on top of their method results in a validation accuracy of 40% (3.7% improvement) and a test accuracy of 36.89% (3.3% improvement). This sets a new SOTA result for differentially private training on the ImageNet-1k dataset.

Ablation study: We conduct ablation studies on the choice of the hyper-parameters of DiSK, specifically, how κ, γ impact the algorithm performance. In Figure 8, we plot the accuracy on different combinations of (κ, γ) , and (κ, ϵ) . We observe a clear trend of performance change for different combinations of the parameters, and there is an optimal choice of κ, γ for different ϵ 's.

C.4 ADDITIONAL EXPERIMENTS ON NLP TASKS

In this section, we provide additional results for NLP tasks.

Parameter-efficient fine-tuning on GLUE. We fine-tune a RoBERTa-base and a RoBERTa-large model from the Huggingface checkpoints² on the GLUE dataset. We follow the same training scripts

²<https://huggingface.co/FacebookAI/roberta-base>, <https://huggingface.co/FacebookAI/roberta-large>

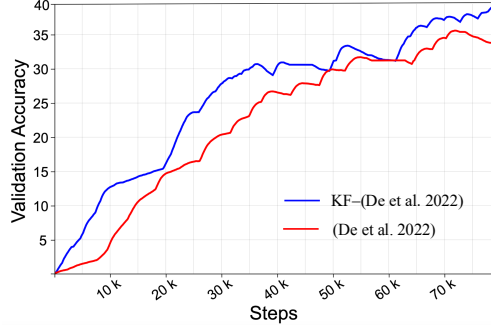


Figure 7: Comparison with the SOTA approach in De et al. (2022) on the ImageNet-1k dataset.

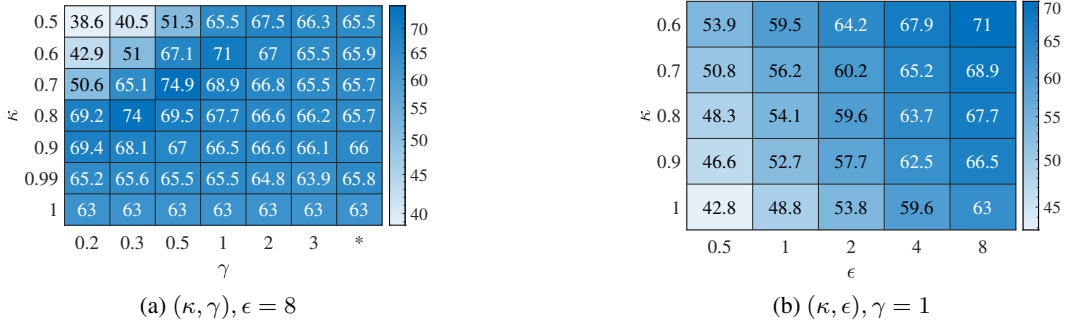


Figure 8: Test accuracy for different combinations of the hyper-parameters when training CNN on the CIFAR-10 dataset.

in Bu et al. (2024) on the hyper-parameter choices of η, B, E on the tasks and use rank $r = 16$ for LoRA. We choose $\kappa = 0.7, \gamma = 0.5$ for DiSK. The results are listed in Table 3. With privacy budget $\epsilon = 1, 6.7$, DPLoRA with DiSK significantly outperforms SOTA results with vanilla DPLoRA on all tasks.

Table 3: Test accuracy of fine-tuning result on the GLUE dataset.

Algorithm	$\epsilon = 1$				$\epsilon = 6.7$			
	MNLI	QNLI	SST2	QQP	MNLI	QNLI	SST2	QQP
RoBERTa-base								
AdamW ($\epsilon = \infty$)	87.6	92.8	94.8	91.9	87.6	92.8	94.8	91.9
Lora ($\epsilon = \infty$)	87.5	93.3	95.1	90.8	87.5	93.3	95.1	90.8
DPLora	81.1	85.5	90.9	83.9	83.5	87.4	91.5	85.7
KF-DPLora	84.7	90.3	92.9	87.8	85.9	90.5	93.1	89.0
RoBERTa-large								
AdamW ($\epsilon = \infty$)	90.3	94.7	96.4	92.2	90.3	94.7	96.4	92.2
Lora ($\epsilon = \infty$)	90.6	94.9	96.2	91.6	90.6	94.9	96.2	91.6
DPLora	85.6	89.5	90.9	85.1	87.8	90.8	94.3	87.4
KF-DPLora	87.9	92.5	95.2	88.2	89.4	92.6	95.4	89.6

Fine-tuning GPT-2 on text generation tasks. We fine-tune a GPT-2-small model with 137M parameters from the Huggingface checkpoints³ on two text generation datasets, E2E and DART. We follow the same training scripts in Li et al. (2021) on the hyper-parameter choices of η, B, E on the tasks and choose $\kappa = 0.7, \gamma = 0.5$ for DiSK. The results on different metrics for the E2E dataset are given in Table 4, and the results for the DART dataset are in Table 5. With privacy budget $\epsilon = 3, 8$, DPAdamW with DiSK significantly outperforms SOTA results with vanilla DPAdamW on all metrics.

³<https://huggingface.co/openai-community/gpt2>

Table 4: Performance of fine-tuning gpt-2 on the E2E dataset. (All metrics are higher the better)

Algorithm	BLEU (%)	ROUGE-L (%)	METEOR	NIST	CIDEr
AdamW ($\epsilon = \infty$)	69.46	71.36	0.461	8.780	2.422
DPAdamW ($\epsilon = 3$)	61.52	65.87	0.417	7.071	2.167
KF-DPAdamW ($\epsilon = 3$)	68.35	70.23	0.456	8.636	2.399
DPAdamW ($\epsilon = 8$)	64.99	67.34	0.425	8.387	2.192
KF-DPAdamW ($\epsilon = 8$)	68.73	70.58	0.460	8.697	2.463

Table 5: Performance of fine-tuning gpt-2 on the DART dataset. Val. Perp. stands for validation perplexity. (All metrics except Val. Perp. are higher the better)

Algorithm	Val. Perp. ↓	BLEU (%)	ROUGE-L (%)	METEOR	NIST	CIDEr
AdamW ($\epsilon = \infty$)	0.921	44.56	58.66	0.379	8.733	2.773
DPAdamW ($\epsilon = 3$)	1.427	33.96	52.38	0.310	6.090	1.864
KF-DPAdamW ($\epsilon = 3$)	1.149	41.01	57.53	0.359	7.949	2.553
DPAdamW ($\epsilon = 8$)	1.362	35.30	54.58	0.320	6.365	1.995
KF-DPAdamW ($\epsilon = 8$)	1.102	42.12	58.11	0.364	8.111	2.628

C.5 IMPROVEMENT OVER SOTA

In the following Table 6, we provide a list of the experiment settings where our algorithm outperforms SOTA results. The paper that provides the SOTA results is cited for each setting, or the same as the line above. We observe that DiSK provides new SOTA for CV datasets, including CIFAR-10, CIFAR-100, and ImageNet-1k, and NLP datasets, including GLUE (MNLI, QNLI, QQP, SST-2), DART, and E2E.

Table 6: Comparison with SOTA, PT=pre-training, FT=fine-tuning.

Dataset	TASK	Model	ϵ	Ours (%)	SOTA (%)
CIFAR-10	PT	CNN	0.5	59.7	N/A
CIFAR-10	PT	CNN	2	68.8	67.2 (Tramer & Boneh, 2020)
CIFAR-100	PT	WRN	0.5	14.7	N/A
CIFAR-100	PT	WRN	1	22.7	14.1 (Bao et al., 2024)
CIFAR-100	PT	WRN	2	30.0	21.5
CIFAR-100	PT	WRN	4	37.1	33.3
CIFAR-100	PT	WRN	8	42.0	40.6
CIFAR-100	FT	ViT	0.5	83.49	78.3 (Mehta et al., 2023)
CIFAR-100	FT	ViT	1	85.36	81.8 (Bao et al., 2024)
CIFAR-100	FT	ViT	2	86.77	83.5
CIFAR-100	FT	ViT	4	87.56	84.5
CIFAR-100	FT	ViT	8	88.49	84.6
ImageNet-1k	PT	ViT	8	40.00	36.35 (De et al., 2022)
MNLI	FT	RoBERTa-base	1	84.7	83.2 ($\epsilon = 3$) (Bu et al., 2023)
QNLI	FT	RoBERTa-base	1	90.3	87.4 ($\epsilon = 3$)
QQP	FT	RoBERTa-base	1	87.8	85.8 ($\epsilon = 3$)
SST-2	FT	RoBERTa-base	1	92.9	92.3 ($\epsilon = 3$)
MNLI	FT	RoBERTa-base	6.7	85.9	83.8 ($\epsilon = 8$) (Bu et al., 2023)
QNLI	FT	RoBERTa-base	6.7	90.5	87.9 ($\epsilon = 8$)
QQP	FT	RoBERTa-base	6.7	89.0	86.6 ($\epsilon = 8$)
SST-2	FT	RoBERTa-base	6.7	93.1	93.0 ($\epsilon = 8$) (Li et al., 2021)
MNLI	FT	RoBERTa-large	1	87.9	86.8 (Yu et al., 2021)
QNLI	FT	RoBERTa-large	1	92.5	88.0
QQP	FT	RoBERTa-large	1	88.2	85.2
SST-2	FT	RoBERTa-large	1	95.2	93.1
MNLI	FT	RoBERTa-large	6.7	89.4	89.0 (Yu et al., 2021)
QNLI	FT	RoBERTa-large	6.7	92.6	92.5
QQP	FT	RoBERTa-large	6.7	89.6	88.4

Dataset	TASK	Model	ϵ	Ours (%)	SOTA (%)
SST-2	FT	RoBERTa-large	6.7	95.4	95.3
E2E (BLEU)	FT	GPT-2	3	68.35	61.52 (Li et al., 2021)
E2E (ROUGE-L)	FT	GPT-2	3	70.23	65.87 (Bu et al., 2024)
E2E (BLEU)	FT	GPT-2	8	68.73	63.60 (Bu et al., 2024)
E2E (ROUGE-L)	FT	GPT-2	8	70.58	67.53 (Li et al., 2021)
DART (BLEU)	FT	GPT-2	3	41.01	32.33 (Li et al., 2021)
DART (ROUGE-L)	FT	GPT-2	3	57.53	52.06
DART (BLEU)	FT	GPT-2	8	42.12	35.06
DART (ROUGE-L)	FT	GPT-2	8	58.11	54.57